AD-A152 318 CONSTRUCTION AND ANALYSIS OF A PRIZ SPATIAL LIGHT MODULATOR EXHIBITING DY..(U) AIR FORCE INST OF TECH WRIGHT-PATTERSON AFB OH SCHOOL OF ENGI.. D M SHIELDS 1/1

UNCLASSIFIED DEC 84 AFIT/GEO/ENP/84D-4 F/G 20/6 NL

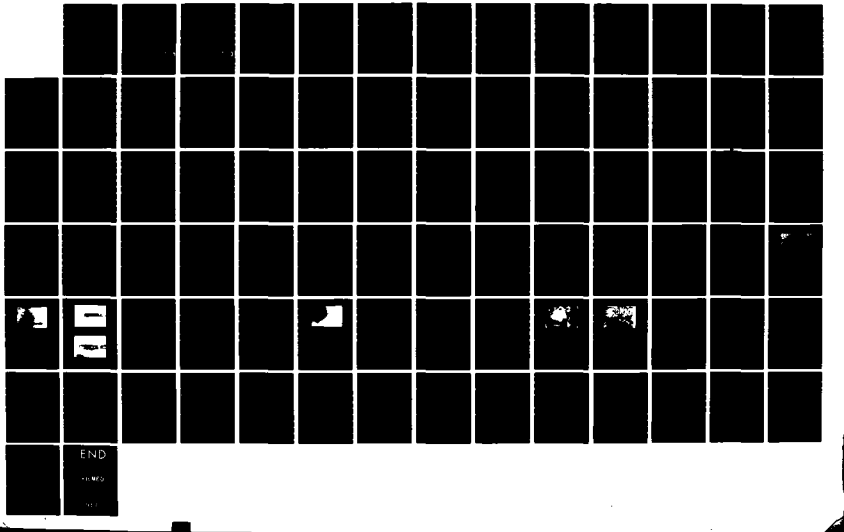

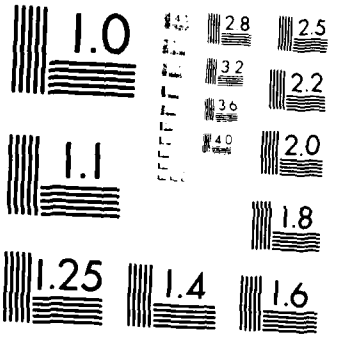

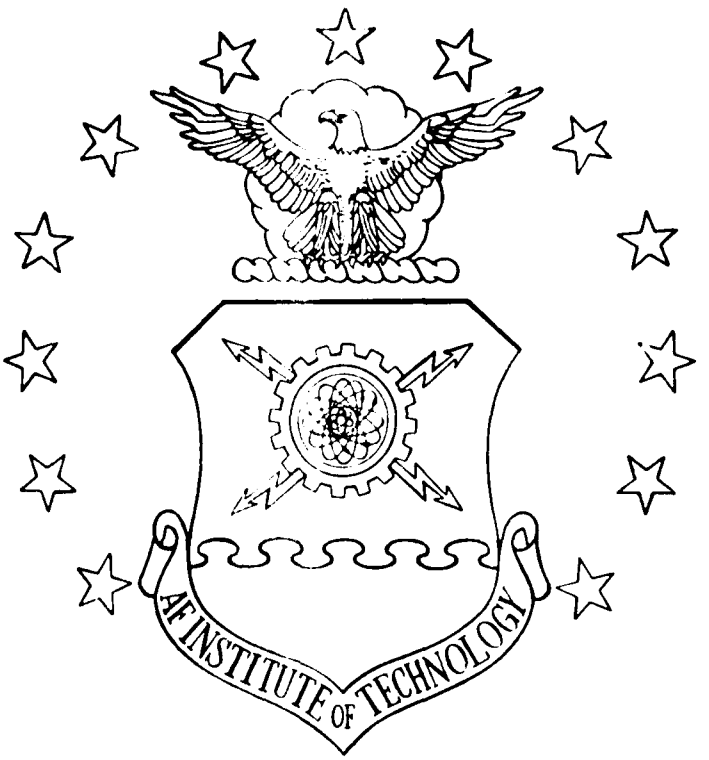

CONSTRUCTION AND ANALYSIS OF A PRIZ SPATIAL LIGHT MODULATOR EXHIBITING DYNAMIC BEAM SELECTION

THESIS

[redacted]
Captain, USAF

AFIT/GEO/ENP/84D-4

DEPARTMENT OF THE AIR FORCE
AIR UNIVERSITY
AIR FORCE INSTITUTE OF TECHNOLOGY

Wright-Patterson Air Force Base, Ohio

AFIT/GEO/ENP/84D-4

CONSTRUCTION AND ANALYSIS OF A PRIZ SPATIAL LIGHT MODULATOR EXHIBITING DYNAMIC IMAGE SELECTION

THESIS

Duncan H. Sheets
Captain, USAF

AFIT/GEO/ENP/84D-4

Approved for public release; distribution unlimited

AFIT/GEO/ENP/84D-4

CONSTRUCTION AND ANALYSIS OF A PRIZ SPATIAL LIGHT MODULATOR EXHIBITING DYNAMIC IMAGE SELECTION

THESIS

Presented to the Faculty of the School of Engineering
of the Air Force Institute of Technology
Air University
In Partial Fulfillment of the
Requirements for the Degree of
Master of Science in Electrical Engineering

Duncan M. Shields, B.S.
Captain, USAF

December 1984

Preface

The original proposal for this study was made by my thesis advisor, Dr. Theodore Luke, as a follow-on to a previous AFIT thesis. That thesis centered on the theoretical diffraction efficiency of a new spatial light modulator known as the PRIZ. The PRIZ exhibits many unique capabilities, one being dynamic image selection. Dr. Luke suggested an investigation into this phenomenon.

This investigation required the construction and analysis of a modified current-conducting PRIZ, a task which, as far as published reports indicate, had not been accomplished outside of the Soviet Union.

I would like to thank Dr. Luke for the proposal and for his interest and assistance throughout the project. Mr. Curtis Arnipp provided extensive assistance in all areas of my experimentation. His knowledge, strong back, friendship, and patience enabled me to accomplish my research.

My final and most fervent thanks goes to my wife and children for their strong support during my AFIT tour. The support and love of my family has always been my key to success.

Duncan M. Shields

TABLE OF CONTENTS

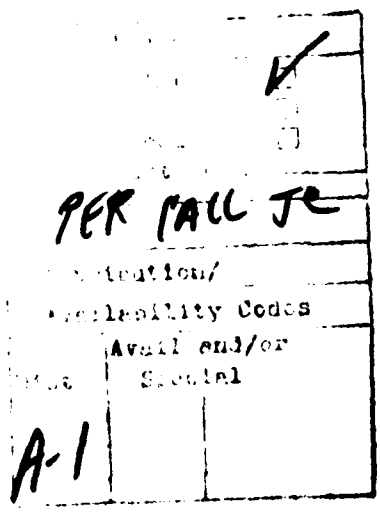

List of Figures

Notation

Roman Letter Symbols

d	-	BSO crystal thickness-mm
d_o	-	Light absorption depth in BSO-cm
$\vec{E}_o$	-	Applied electric field-v/cm
$\vec{E}'$	-	Generalized internal electric field-v/cm
$\vec{E}_R'$	-	Read beam vector
$\vec{E}_t'$	-	Internal transverse electric field
f_{x1}, f_{x2}	-	Spatial frequency-cycles/mm
I_o	-	Incident intensity-W/cm^2
n	-	Index of refraction of BSO
n^I, n^{II}	-	Indices of refraction experienced by ordinary and extraordinary waves
n_i	-	Refractive index of incident media
n_r	-	Refractive index of transmittingmedia
r	-	Electrooptic tensor coefficient for BSO-cm/V
x_1', x_2', x_3'	-	Coordinate system referenced to the (111) face of BSO

Greek Letter Symbols

α	-	Absorption coefficient-cm^{-1}
α''	-	Angle of E_R' with x_1' axis-deg.
γ	-	Angle of E_t' with x_1' axis-deg.
θ_p	-	Polarization angle (Brewsters)-deg.

ρ' - Optical activity coefficient-deg/mm

λ - Wavelength-Angstroms

Γ - Phase change between ordinary and extraordinary waves (through crystal)

Ψ - Rotation of index ellipsoid from x_1' axis-deg

Abstract

A PRIZ electrooptic spatial light modulator exhibiting dynamic image selection (current-conducting PRIZ) was constructed, demonstrated, and analyzed.

The current-conducting PRIZ was constructed by vacuum depositing transparent chromium electrodes on the large faces of a thin (0.5 mm) slice of (111) cut Bismuth silicon oxide ($Bi_{12}SiO_{20}$ or BSO).

Dynamic image selection was demonstrated by writing a stored image into the device with an Argon ion laser and erasing the image reproduced by a circularly polarized HeNe laser readout beam. This experiment verifies the dynamic image selection effect with a device constructed outside of the Soviet Union, an accomplishment not previously reported.

The BSO material was analyzed and found to exhibit optical activity and refractive index values similar to other electrooptic crystal material. The conductivity and absorption coefficients differed significantly from the published results, being higher and lower, respectively.

The experimental device exhibits directional filtering in agreement with published theory and also exhibits optical image times of up to 70 minutes.

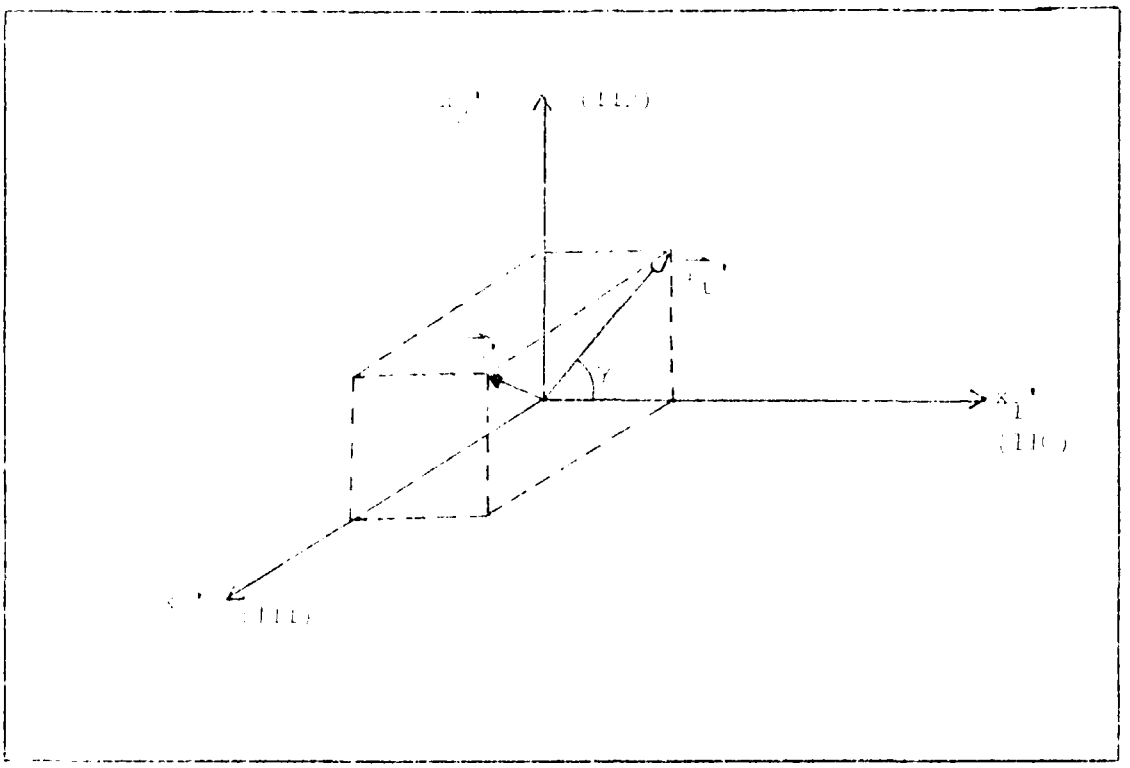

Fig. 6. Selected Coordinate System and Electric Fields in (111) (crystallographic direction) PRIZ (32)

Chapter II lists the electrooptic coefficient as 5×10^{-10} cm/V. The equality of the three non-zero elements indicate the crystal is isotropic under no-field conditions. Therefore, to use this device as a spatial light modulator, transverse electric fields must be created within the device. The origin of these internal electric fields will be discussed in the next section.

The specific techniques used to obtain the plane wave [illegible] through BSO are rigorously described [illegible] by Roggeman (31). The specific [illegible] device ((111) crystal cut) is used as [illegible] describes the specific modu-

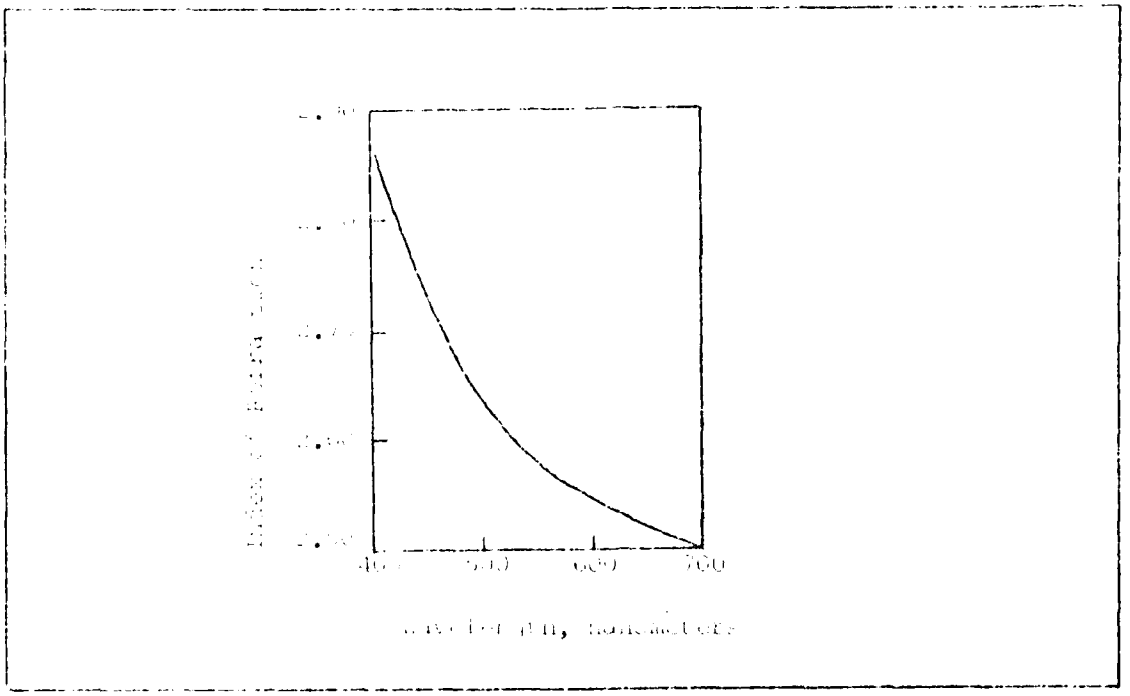

Fig. 6. Index of Refraction (n) versus Wavelength (λ)
for Ice (2:493)

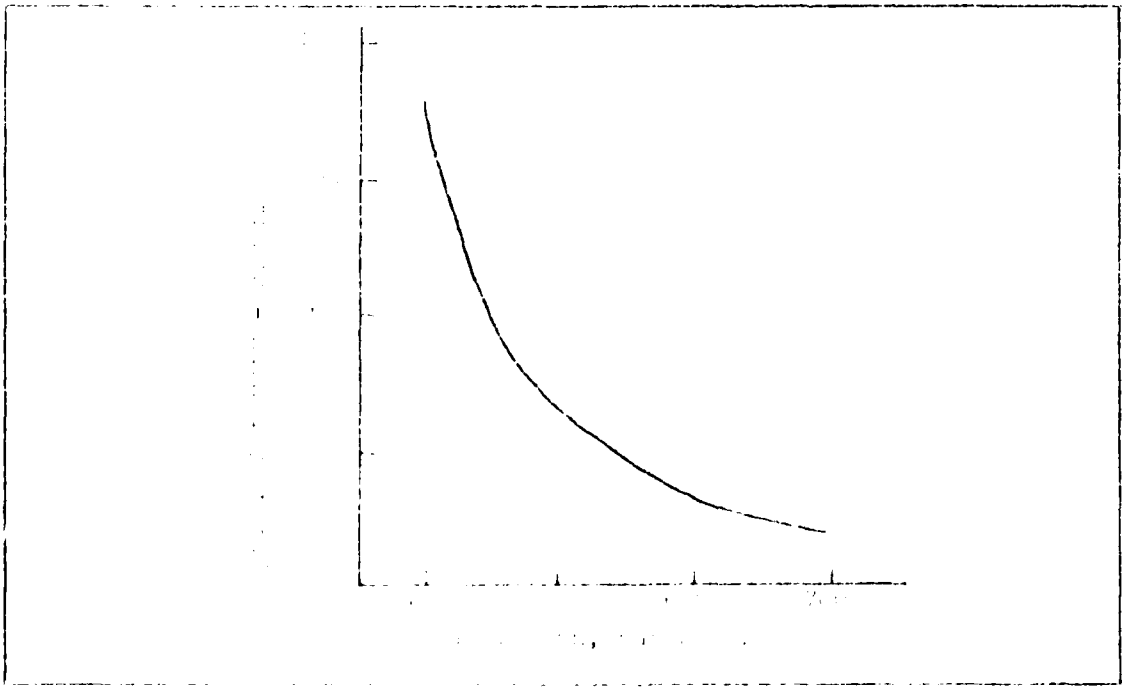

Fig. 7. [illegible] versus Wavelength (λ)

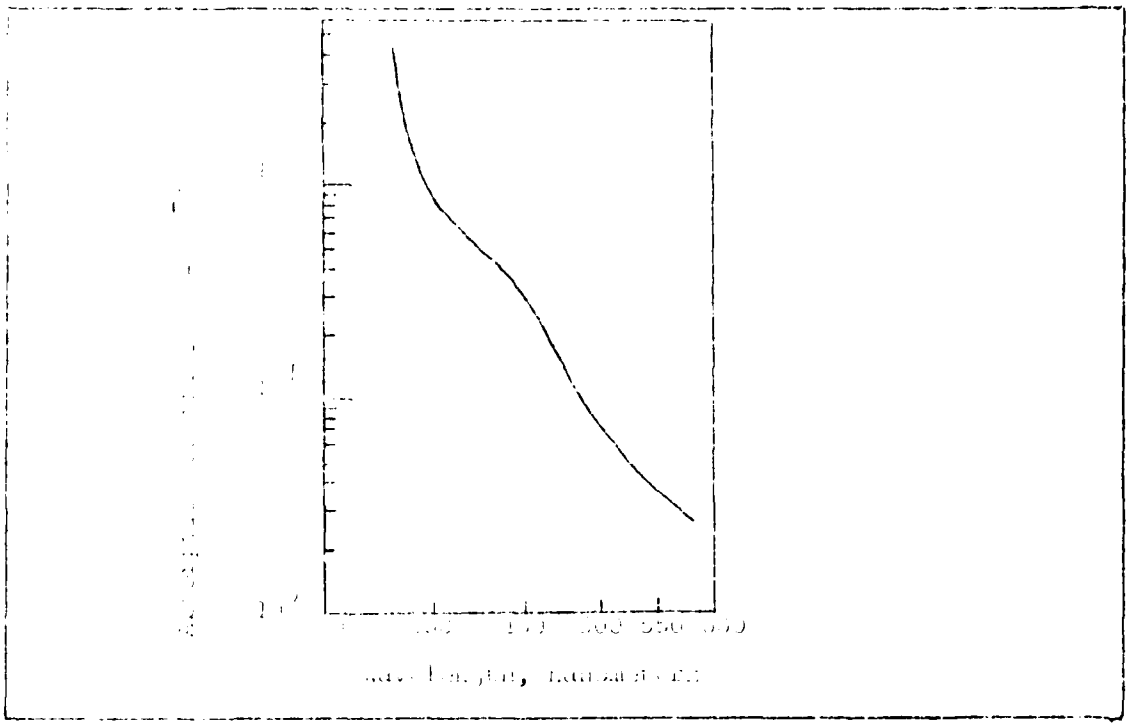

Fig. 4. Absorption Coefficient (α) versus Wavelength (λ) for 850 (34:1673)

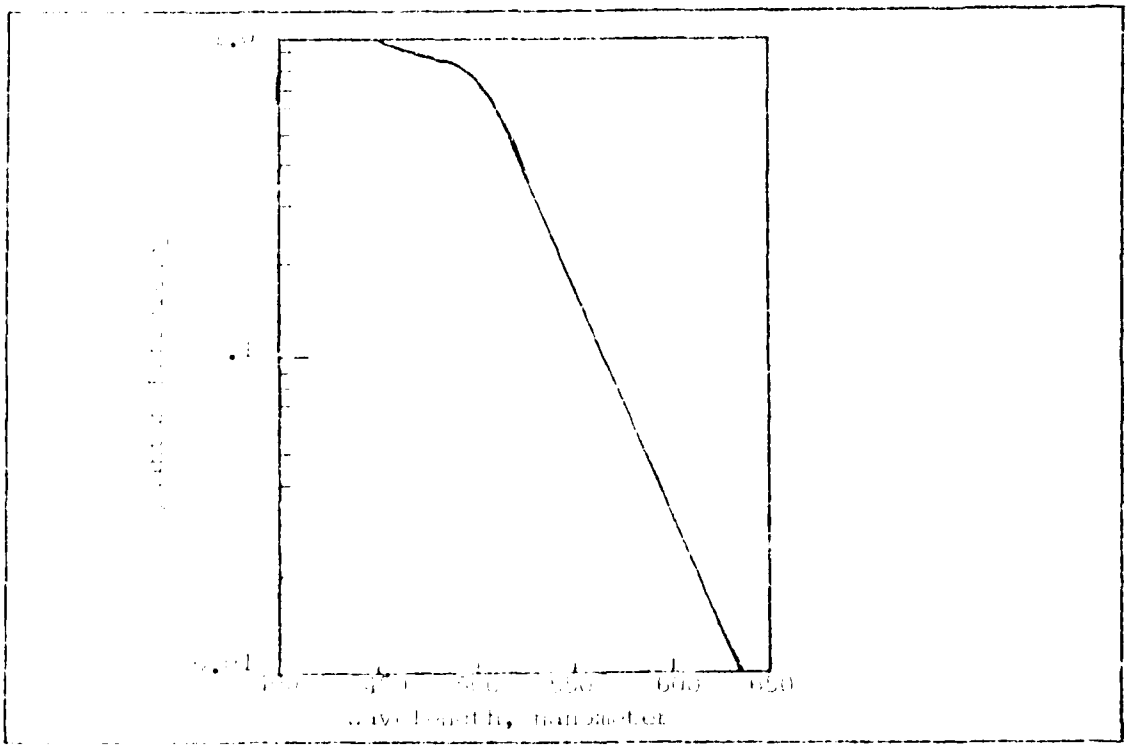

Fig. 5. Quantum Efficiency versus Wavelength (λ) for 850 (34:1677)

density and energy levels of the traps and donors (21:246).

The wavelength dependent nature of several material parameters of BSO, such as the absorption coefficient and quantum efficiency, are critical to the operation of the PRIZ device. A write-in beam in the blue-green region induces large photorefractive changes while a readout beam in the red causes comparatively little photorefractive change. This capability enhances the PRIZ's use as an ODP element and leads to the experimental geometries described later. Details of the dispersive nature of the absorption coefficient, quantum efficiency, index of refraction, and optical activity are shown in Figures 4 through 7.

Transverse Pockels Effect in BSO

All versions of the PRIZ spatial light modulator utilize the transverse electrooptic effect. This means that an electric field orthogonal to the direction of propagation of read light in the crystal must be present in order to phase modulate the read beam (38:261). BSO was previously noted as being a cubic crystal of crystallographic point-group symmetry 23. This point-group forces the (modified) crystal electrooptic tensor to be of the form:

$$\begin{bmatrix} 0 & 0 & 0 \\ 0 & 0 & 0 \\ 0 & 0 & 0 \\ r_{41} & 0 & 0 \\ 0 & r_{52} & 0 \\ 0 & 0 & r_{63} \end{bmatrix}$$

where $r_{41} = r_{52} = r_{63}$ (38:249).

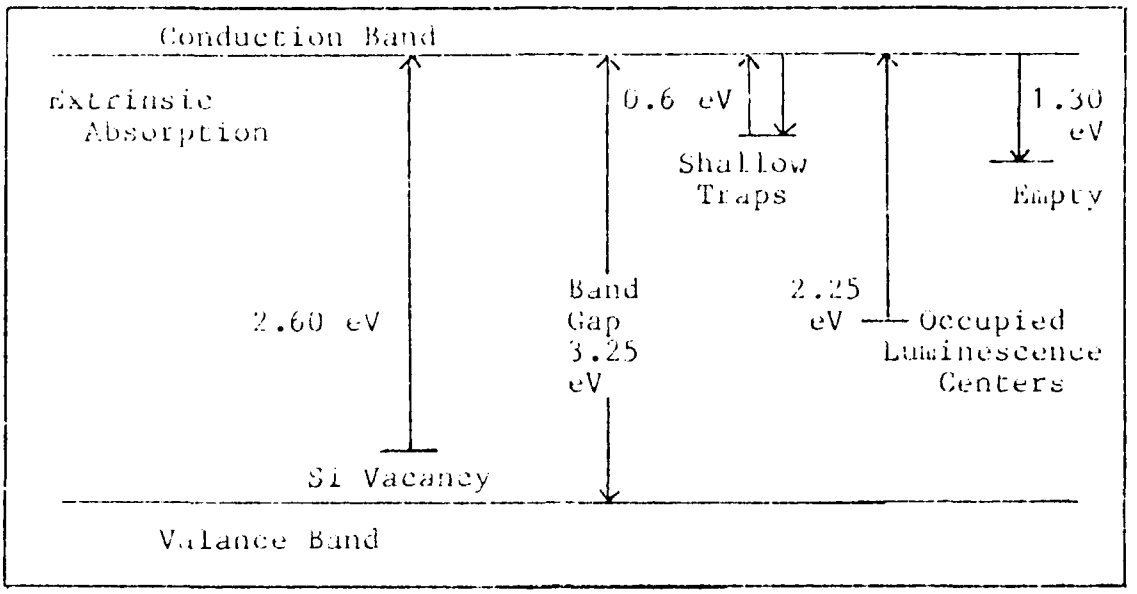

Fig. 3. Energy Band Diagram of Bismuth Silicon Oxide at Room Temperature (23:3684)

The energy band diagram of BSO contains important information on the charge transport mechanism of BSO and its relation to the photorefractive effect. Figure 3 is a diagram of the band structure. The intrinsic bandgap of the material is 3.25 ev. The primary donor level is located at 2.60 ev below the conduction band at a density of 10^{19} cm^{-3} and is associated with a silicon vacancy. The trap levels that participate in the charge transfer process are luminescence centers located at 2.25 or 1.30 ev, depending on whether or not the center is electron occupied. These traps have a density of 10^{16} cm^{-3}. A shallow trap at 0.6 ev that may participate in the reduction of the effective mobility of photoelectrons has been identified with a density of 10^{15} cm^{-3}. These measurements are made on nominally pure BSO. BSO is classified as a semi-insulator due to the

wavelength, are upon migration, retrapped at other locations leaving behind positive or negative charges of ionized trap centres. The photo-excited charges will be reexcited and retrapped until they finally drift out of the illuminated region and are trapped. The resulting space-charge field between the ionized donor centres and the trapped charges modulates the refractive indices via the electro-optic effect. Uniform illumination erases the space-charge fields and brings the crystal back to its original state (optical erasure) (14:206).

A summary of some important material characteristics of BSO are shown in Table I.

TABLE I. Physical Parameters of BSO at Room Temperature

Parameter	Value	Unit	Ref.
Point Group Symmetry	23	----	a
Conductivity	20×10^{-15}	$ohm^{-1}cm^{-1}$	a,d
Dielectric Constant	56	----	a,c
Transmission Range	0.45 - 7.5	μm	a
Bandgap	3.25	ev	a,b
Electrooptic Coefficient	5×10^{-10}	cm/V	a,b
Electron Mobility	0.03	$cm^2/V\text{-}s$	c,d
Absorption Coefficient	Figure 4	cm^{-1}	
Quantum Efficiency	Figure 5	%	
Index of Refraction	Figure 6	---	
Optical Activity	Figure 7	deg/mm	

References

a. 2:493
b. 23:3684
c. 36:710
d. 14:214

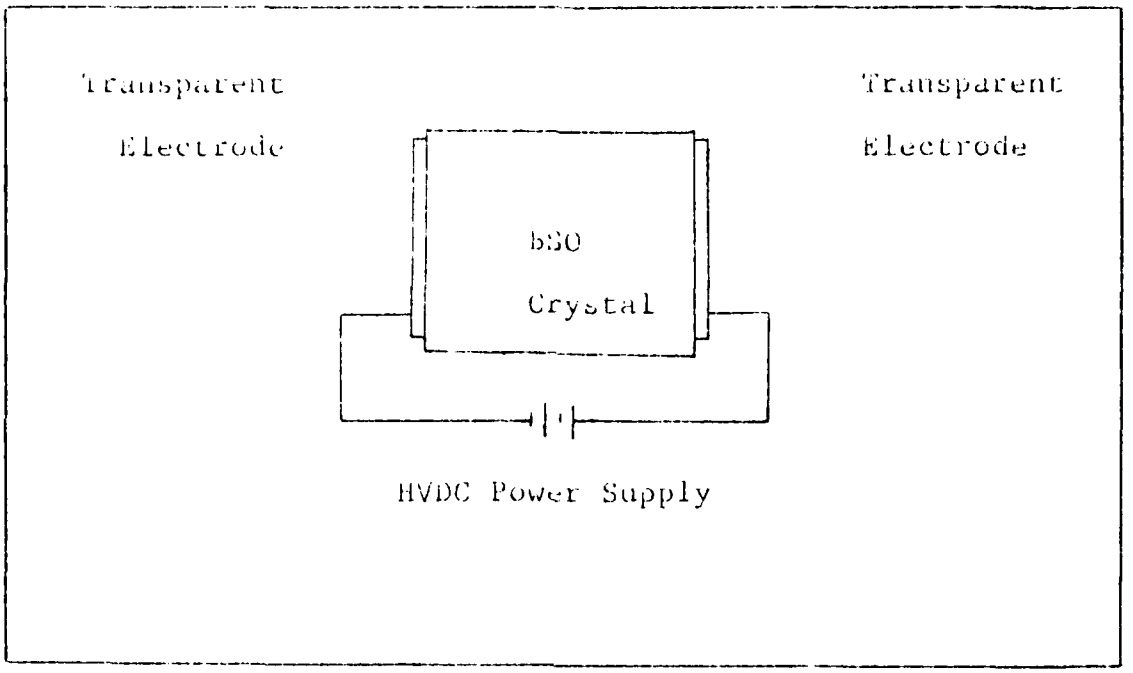

Fig. 2. Modified Current-Conducting PRIZ Structure

the 23 cubic symmetry point group (2:493). BSO is a paraelectric electrooptic photoconductive material with high resistivity. BSO is also optically active. The combination of the linear electrooptic effect, the photoconductivity, and the high dark resistivity results in the photorefractive effect. Photorefraction is light induced changes in the refractive indices (13:470). A capsule version of the photorefractive effect and its general mechanism was stated by Gunter:

> The light-induced changes of refractive indices in electro-optic crystals are based on the spatial modulation of photocurrents by non uniform illumination. The generation of photocurrents at low light intensity depends on the presence of suitable donors, because most of the crystals of interest are inherently transparent in the visible. The electrons or holes, which are excited from the impurity centres by light of a suitable

II. Background and Theory

Current-Conducting PRIZ Structure

The structure of the dynamic image selection PRIZ used for image processing is shown in Figure 2. The device is constructed of a thin (0.3 to 1 mm) slice of single crystal BSO. The large faces of the crystal correspond to the (111) or (110) crystal planes (Miller indices). A similar device, the Pockels Readout Optical Modulator (PROM), utilizes the (100) cut in its construction (12:4216). For the current-conducting PRIZ, transparent metal electrodes of platinum or indium oxide (InO_2) are evaporated directly on the large faces of the crystal (25:162,168). Typical crystal size reported for Soviet devices permitted an active area of 15 mm in diameter at $\lambda/4$ flatness with a 30 mm diameter active area at 1A flatness available (11:3848). The thickness of the electrodes is controlled to provide high conductivity and optical transmissivity. In operation, a constant voltage of 1 to 2 KV is applied between the electrodes. The amount of current conducted through the device during operation is dependent on the dark resistivity and photoconductivity of the material.

BSO Material Parameters

$Bi_{12}SiO_{20}$ (BSO) is a sillenite compound that is grown in single crystal boules by the Czochralski technique. The crystals exhibit a zincblende structure and belong to

theory of the dynamic image selection effect.

Investigation of the material parameters, device construction, device performance, and other observations are covered in Chapter III.

Chapter IV contains a summary of the experimental effort and recommendations for research into the material characteristics, device performance, and theoretical models useful in further development of the device.

development of BSO and the current-conducting PRIZ.

Approach

The problem formulated by this thesis was approached in five phases. The dynamic image selection verification apparatus was designed, assembled, and tested first.

Second, the equipment and techniques necessary to construct the current-conducting PRIZ were assembled and tested. The tasks of this phase consisted of renovating and testing a vacuum apparatus, developing and testing a chromium deposition technique, and developing and testing a mounting procedure for the chromium plated BSO crystal.

The third phase consisted of the actual electrode deposition and mounting of the plated BSO crystal.

The fourth phase involved the verification of the dynamic image selection effect and modification of the experimental apparatus to control and record the effect.

The final phase of the experimental investigation involved design and use of techniques to investigate the material characteristics of BSO and the performance of the current-conducting PRIZ device.

Sequence of Presentation

Background and theory necessary for a good grasp of device operation is presented in Chapter II. This information consists of the structure of the current-conducting PRIZ, a summary of important BSO material parameters, the theory of the transverse electrooptic effect, and the Soviet

constructed as closely as possible to the published Soviet specifications to permit valid comparison of device performance (27:249).

The third section describes the design and construction of an optical test apparatus to verify the dynamic image selection effect, and the verification of that effect. A modification of the apparatus used at CNU for effect demonstration was used in this study (11:3852). The experimental apparatus evolved over the course of the experiment and only the final configuration is shown in this thesis.

The fourth section investigates two interesting device capabilities; spatial filtering and optical memory. The performance of the in-house current-conducting PRIZ for these parameters is compared to the reported performance of the Soviet devices.

The fifth section reports two interesting phenomenon encountered during the experimental effort. Laser-induced damage to the BSO crystals was encountered on two occasions. The constructed PRIZ device also exhibited light and current oscillations of varying rates depending on the time, write-light intensity, and field voltage. These phenomenon were not analyzed, but were reported to provide a more complete picture of the experimental effort and to identify these occurrences for future investigators.

The last section summarizes the experimental effort and suggests additional avenues for experimental and theoretical

Union.

Problem

The purposes of this study were to investigate the material characteristics of BSO supplied by an American company, construct a current-conducting PRIZ, design an experiment that could verify the phenomenon of dynamic image selection and investigate the performance of an in-house device.

Scope

This study is divided into six sections. The first section involves the investigation of four material characteristics:

1. optical activity
2. index of refraction
3. absorption coefficient
4. conductivity

The experiments were designed and conducted to investigate the wavelength dependent nature of the first three characteristics and compare them to published results. The last characteristic, conductivity, was investigated to obtain data on the current versus voltage response of the purchased BSO material. This information was also compared to published results. All published BSO material investigations referenced in this thesis were conducted by American researchers. The Soviet literature reviewed references only American studies when they list a material parameter.

The second section describes the actual design and construction of a current-conducting PRIZ. The device was

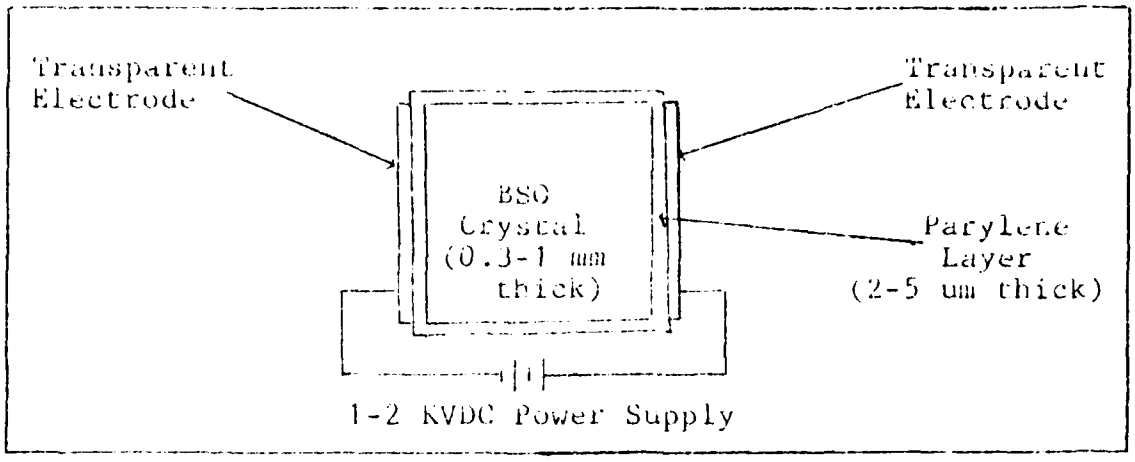

Figure 1. PRIZ Configuration

inal E-O effect (24:790). This device has demonstrated 10 times greater resolution and efficiency than concurrently rated PROM devices (12:4220).

The PRIZ (in a specific configuration) also exhibits an effect, similar to time differentiation of an image, that the Soviets have labeled "dynamic image selection" (30:165). The device rejects the constant or nonvarying parts of an image and modulates the readout beam with the time varying parts of the image. The specific (current-conducting) configuration of the PRIZ that exhibits dynamic image selection is identical to Figure 1 except that the parylene layers have been removed.

The dynamic image selection phenomenon was initially reported in the Soviet literature and later demonstrated using Soviet devices at Carnegie-Mellon University (CMU) (11:3851). To date, there are no formal reports available verifying this effect with devices made outside the Soviet

CONSTRUCTION AND ANALYSIS OF A PRIZ SPATIAL LIGHT MODULATOR EXHIBITING DYNAMIC IMAGE SELECTION

I. Introduction

Optical data processing architectures operate by modifying data over a 2-dimensional plane in real-time. The mathematical techniques for this type of optical parallel processing date from the 19th century, while the specific architectures have been extensively developed over the past 20 years (18:10). The limiting factor in the development of optical data processing (ODP) is the technology of the input, output, and processing transducers. These optical elements must be able to spatially modulate a 2-dimensional optical field in real time.

One highly promising spatial light modulator (SLM) device is known as the PRIZ, a Russian acronym for Preobrasovatel Izobrazheniya, meaning Image Transducer (11:3846). The PRIZ is similar to the well-known Pockels Readout Optical Modulator (PROM) as it is cut from Bismuth Silicon Oxide (BSO) and uses the electrooptic (E-O) effect to spatially phase modulate a readout beam. The PRIZ, like the PROM, is constructed in a layered fashion (25:162-163). Figure 1 illustrates the structure of the PRIZ. The PRIZ, however, is cut in a different, (110) or (111) instead of (100), crystal direction, and utilizes the transverse rather than longitud-

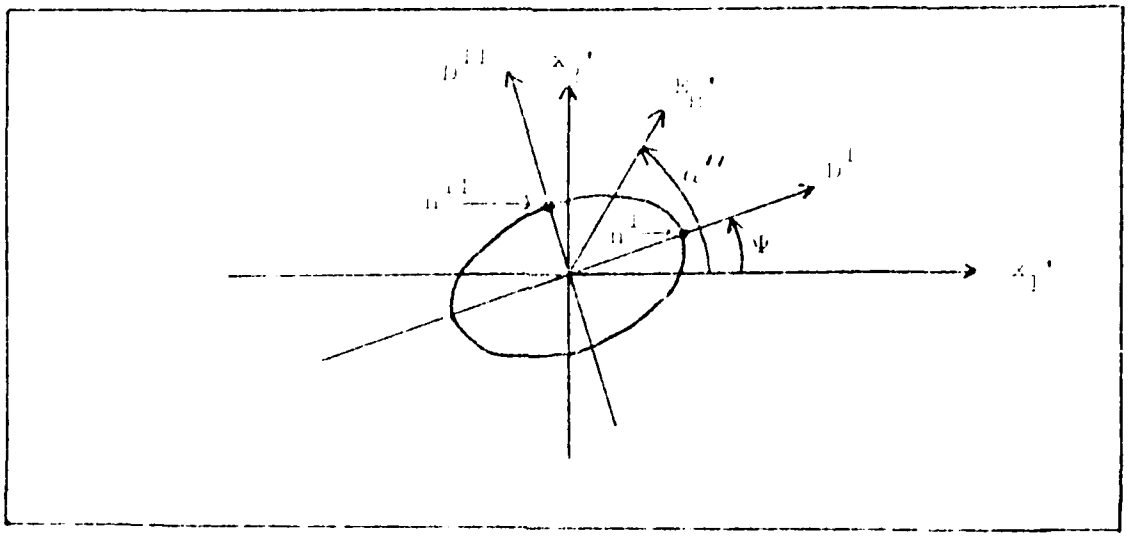

Fig. 9. Index Ellipsoid Representation of Plane Wave Solutions in (111) PRIZ (31)

lation effect of the device upon an incident read beam. Figure 8 shows the coordinate system used for the (111) crystal orientation. $\vec{E}'$ represents a generalized internal electric field (transverse and longitudinal components) while $\vec{E}_t'$ is the projection of the internal field on the plane normal to the propagation direction. γ is the angle of the internal transverse field with the x_1' axis or (110) crystallographic direction. One of the important aspects of PRIZ operation is that the modulation effect is due only to the transverse fields. The fact that the longitudinal field (x_3' direction) has no influence on the eigenvectors or eigenvalues of the plane wave solutions permits a 2-dimensional geometric solution (in the form of the index ellipsoid) to be used for solution. The cross section of the index ellipsoid normal to the direction of propagation is shown in Figure 9. The major (D^1) and minor

($n^{\perp}$) axes of the cross section correspond to the eigenvectors while the lengths of the axes, $n^{\perp}$ and $n^{\parallel}$, correspond to the eigenvalues. Ψ is the rotation angle of the eigenvectors from the x_1' axis due to the orientation of the internal transverse electric field $\vec{E}_t'$. It has been shown (24:790) that the relationship between the two angles is simply:

$$2\Psi = \pi/2 - \gamma$$

Note that the magnitude of the internal field has no effect on the orientation of the index ellipsoid.

Also of primary interest is the phase difference between the eigensolutions after propagation through the crystal. The phase difference is,

$$\Gamma = (2\pi/\lambda)(2/3)^{1/2} n^3 r E_t' d$$

The $\vec{E}_t'd$ term is actually the integrated effect of the transverse electric field through the volume of the crystal. It should be replaced by,

$$\int_0^d \vec{E}_t'(x_3')\,dx_3'$$

The form of $\vec{E}_t'(x_3')$ is quite complex and based on light absorption and charge transport within the crystal (4:65). A qualitative description of the process is presented in the next section.

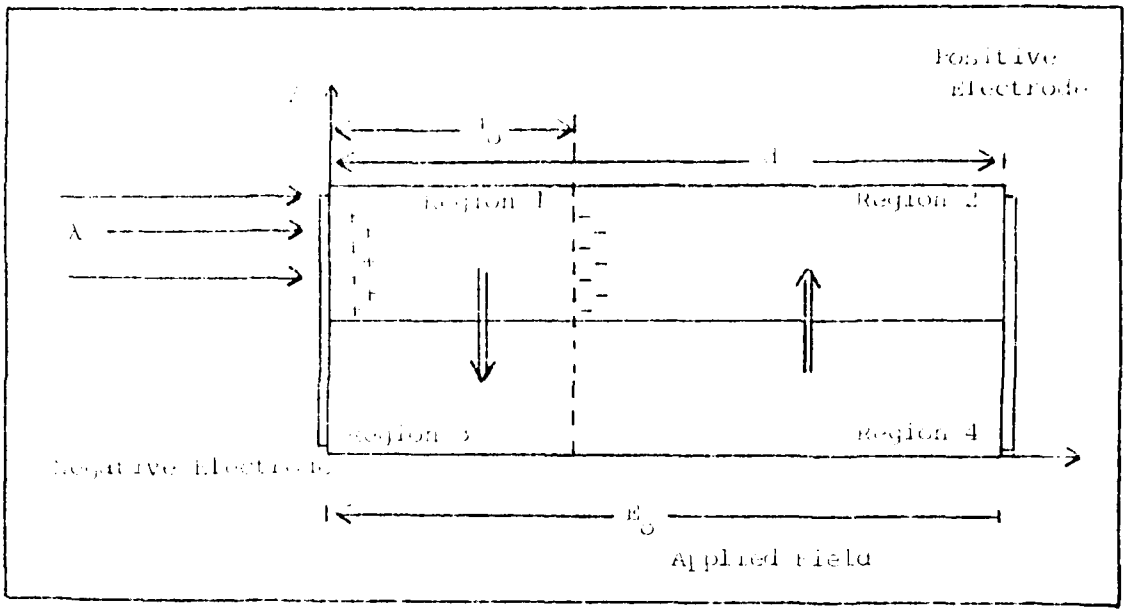

Fig. 10. Cross-Sectional View of Electric Fields and Space Charge in the Current-Conducting PRIZ (10:193)

Dynamic Image Selection

The dynamic image selection feature of the PRIZ device was reported in the Soviet Union in 1980 (30:3165) and later verified by Casasent in 1981 using Soviet devices (12:3851). This section contains phenomenological descriptions, via the Soviet literature, of the establishment of the internal fields in the current-conducting PRIZ based on a band transport model. Also included are the reported performance of Soviet devices with regard to time and input spatial frequency, and the visual manifestation of the dynamic image selection effect.

The energy band diagram for BSO was described in Chapter II, and the accompanying diagram, Figure 3, may be helpful in the following discussion. Figure 10 illustrates the establishment of the internal fields in a cross-

sectional view of the current-conducting PRIZ.

The internal fields are established by a superposition of two mechanisms. First, the longitudinal field is impressed as shown in Figure 2 by the application of a DC voltage between the front and back of the crystal (negative electrode on the illuminated side). This initial condition sets the stage for the buildup and decay of the internal E-fields. Second, illumination of the crystal causes the establishment of the transverse fields. The buildup and decay of these fields can be described in a series of four stages.

In Stage 1 the incident light, with photon energy sufficient (~ 2.6 ev) to excite an electron from a donor site, creates an ionized donor-electron pair at the site of excitation. The distance d_o corresponds to complete (to the 1/e point) absorption of the incident light where $d_o = \alpha^{-1}$ and α is the coefficient of absorption for the incident light. Stage 2 is the separation of charge as the electron drifts into the bulk of the crystal due to the external E-field, $\vec{E}_o$, and the ionized donor remains trapped at the excitation site creating a net positive ionic space charge in Region 1 (i0.193). Stage 3 involves the trapping and release of the photoelectrons by shallow traps which decreases the effective mobility and creates a negative ionic space charge within the bulk of the crystal (Region 2). The form of the electric fields based on

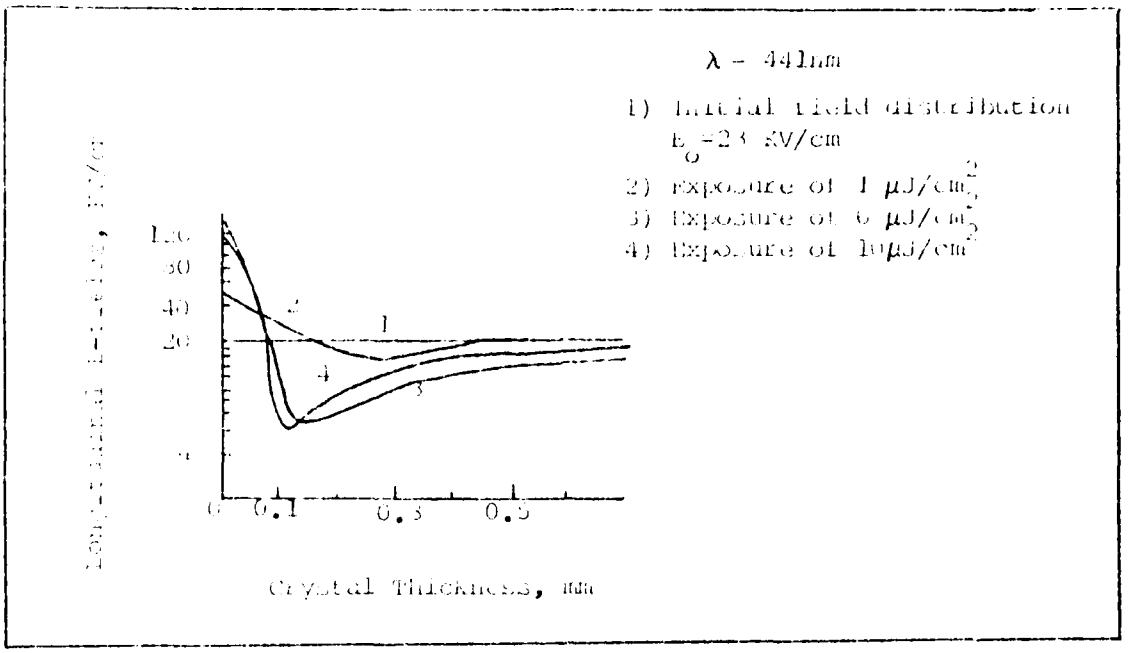

Fig. 11. Longitudinal Electric Fields in BSO for Various Levels of Recording Light (fixed λ) (9:165)

Soviet experimentation) within the crystal for several levels of recording light exposure is shown in Figure 11. The region where the E-field magnitude dips to its lowest value is called a "bottleneck" (8:30). Since the velocity of the photoelectrons in the conduction band is the product of the electric field and the electron mobility, the effective velocity of the electrons decreases in the region of the dip. This decrease in velocity results in the trapping of virtually all of the photoelectrons in the vicinity of the bottleneck and the formation of a negative ionic space charge in the region beyond the bottleneck. As more photoelectrons are generated, the field minimum will move toward the illuminated negative electrode because the positive charge density near the electrode continues to increase

(disregarding saturation) (9:1o5).

The charge distribution created by the incident photons is treated at a point in the above analysis. If the illumination on the surface of the device is inhomogeneous or spatially modulated (an image), then the longitudinal field distribution and space charge density will be different at each point depending on the spatial intensity variation of the recording light. The spatial variation in the space charge density generates transverse fields. This transverse field causes modulation of a readout beam due to the transverse Pockels effect. Region 3 corresponds to a non-illuminated section of crystal surface. The net electric fields between Regions 1 and 3, and 2 and 4 during Stage 3 are shown by the solid arrows.

Stage 4 of the internal field process involves the decay of the internal fields and therefore is the heart of the dynamic image selection effect. If at this point, the recording light is switched off, diffusion and drift due to the non-uniform charge distribution will reduce the assymetry in the longitudinal fields effectively erasing the recorded input pattern. If the recording light is not switched off, diffusion and drift of electrons in the band from Regions 1 to 3, and 2 to 4 will tend to equalize the charge differential between the illuminated and nonilluminated regions. A more prominent driver of this equalization is the excess of carriers available in the conduction band from continued photoproduction and from the dark current. The

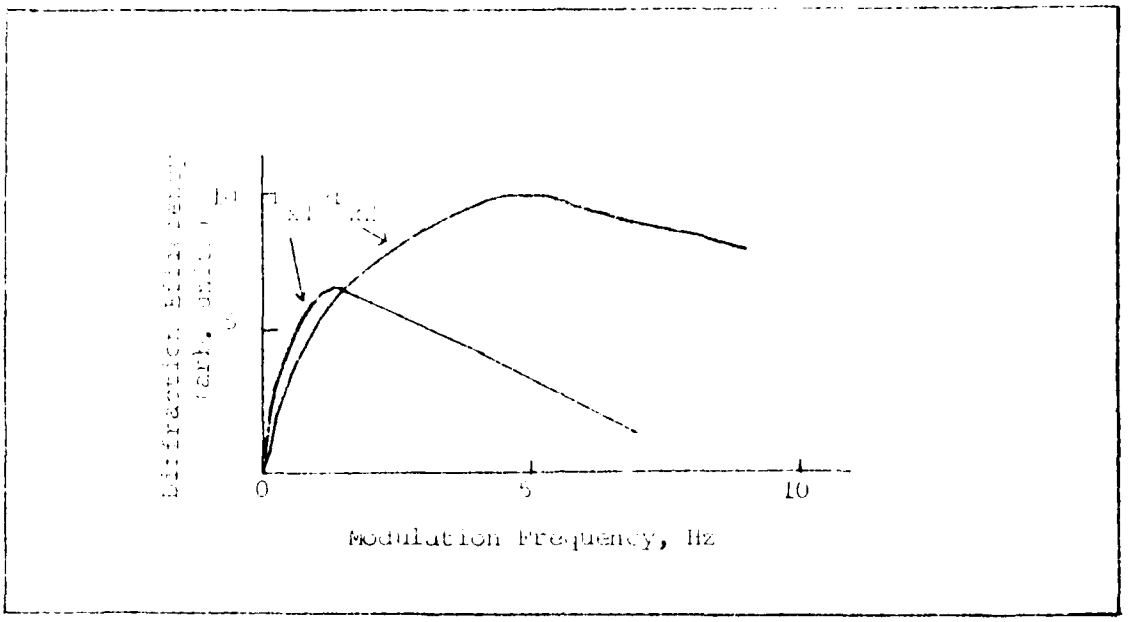

Fig. 12. Diffraction Efficiency of Soviet PRIZ vs Temporal and Spatial Frequency (30:165)

result of the charge homogenization process is to cause the electrooptically produced image to fade with time. The fading, or erasure of the input image is faster if the recording light is left on than when it is turned off (for short write-in times), due to erasure by the write beam.

The spatial and temporal performance of the PRIZ is quantified by the Soviets and other researchers by measuring thediffraction efficiency of the device. The diffraction efficiency is defined as the percentage of incident read light intensity diffracted into either of the first order maxima (not both) by a sinusoidal index grating written into the PRIZ device (31:87). An example of the dependence of diffraction efficiency in the current-conducting PRIZ on spatial and temporal frequencies is shown in Figure 12. The curve representing the higher spatial frequency, labeled

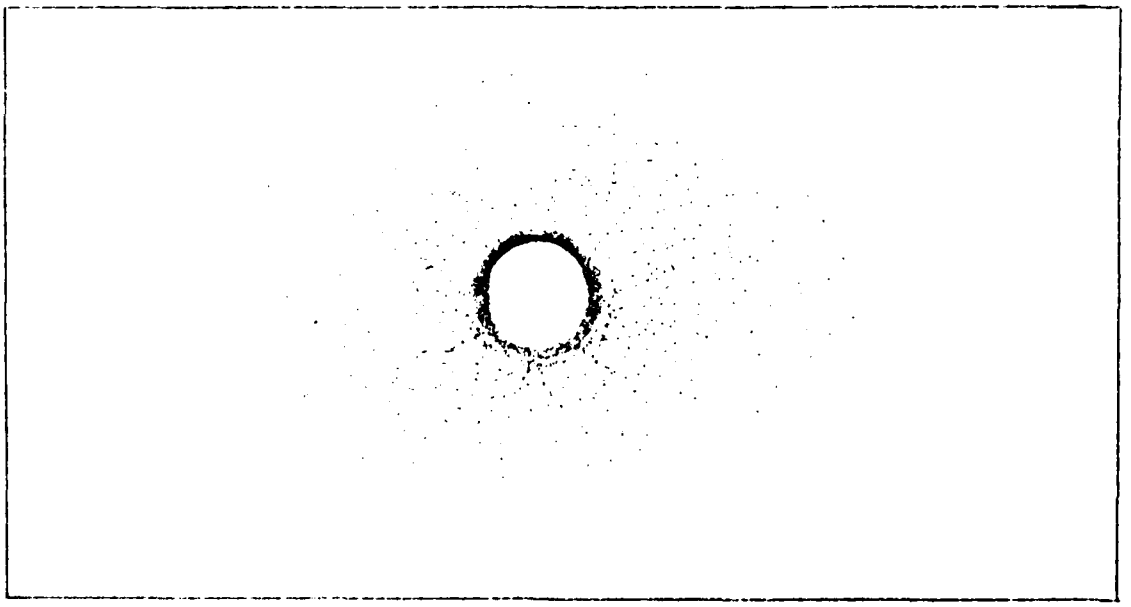

Fig. 13. Edge-Enhanced Output Image of Input Spot

f_{x1}, shows a lower peak diffraction efficiency. This peak occurs at a lower temporal frequency as well, and demonstrates the observed relation between spatial and temporal frequencies with regards to device performance.

The final result of parameters discussed above is best described by an example. If an image consisting of a spot is written into the device, the output will consist of an edge-enhanced version of the input spot. Figure 13 is a diagram of what is actually seen with the darkest areas corresponding to the most light output (like a photographic negative). In a similar manner, any complex image will have a bright band of light associated with any edge between the light and dark areas. Any homogeneously light or dark regions of the input image will not be reproduced in the output (zero suppression). This image will fade to nonvisi-

bility within 1-2 seconds. The time for the image to fade to nonvisibility was observed (but not quantified) to be dependent on the intensity of the write light and magnitude of the longitudinal E-field. If the write-in image is moved, the edges of the output image will show an increased brightness as the write-in image is moved. The magnitude of the light output is dependent on the speed, spatial frequency, and write beam intensity. The observed result with a moving image is that it can be spatially tracked by the increased light output along the direction of movement.

III. Experiment

Material Characteristics Investigation

The purpose of the material (BSO) characteristics investigation was to determine the similarities and differences between the bSO samples used in this experiment and the BSO used in other material studies. The growth of BSO crystals by the Czochralski method is considered to be an art rather than a science. Each boule is different. Since the optical properties of the material determine the performance of the finished device, it is imperative to investigate each sample to be able to predict the performance of the finished device. Ultimately a correlation between the impurity energy levels and densities, optical properties, and performance of the current-conducting PRIZ will lead to a reliable theoretical model of its operation. The specific material characteristics investigated in this study are optical activity, index of refraction, absorption coefficients, and conductivity. The experimental results are compared to American published figures for BSO.

Optical Activity.

Experimental Apparatus. The equipment arrangement for the measurement of optical activity is shown in Figure 14. The laser source (Spectra Physics 126 Argon ion or Spectra Physic 125A Helium Neon) is vertically polarized and the crystal, analyzer, and radiometer probe (EG&G 450) are

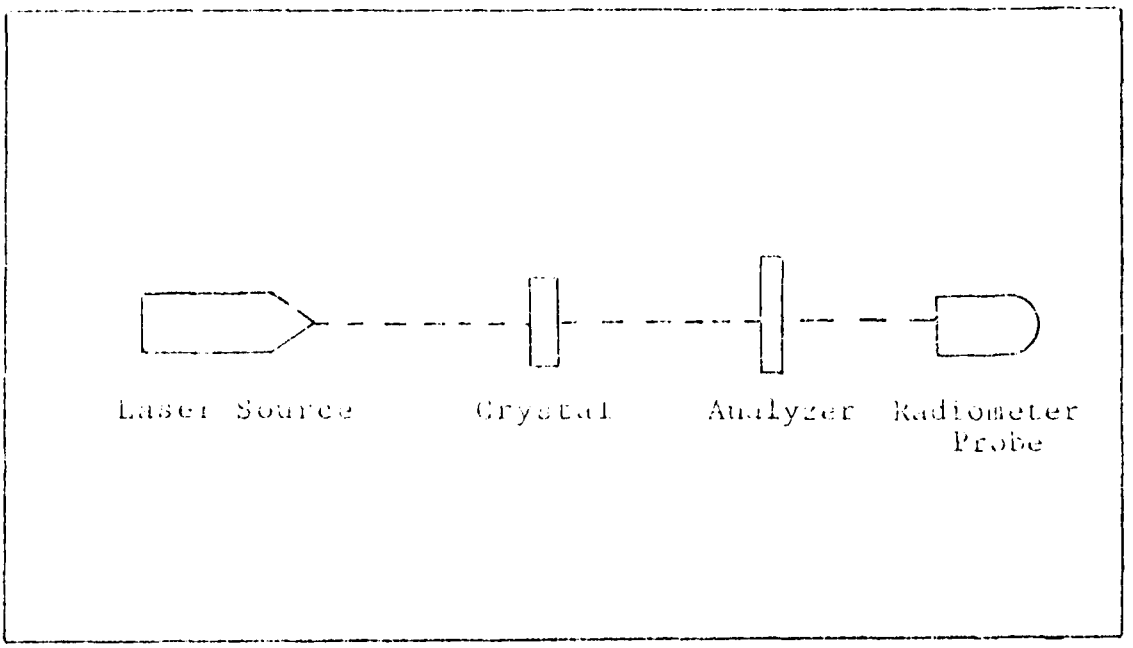

Fig. 14. Optical Activity Measurement Apparatus

normal to the laser beam propagation. The analyzer is mounted in a calibrated rotating ring.

Experimental Procedure. With the crystal absent from the beam path, the analyzer is rotated to provide a minimum reading on the radiometer. The crystal is then placed in the beam path and the analyzer rotated to achieve a minimum radiometer reading. The magnitude and direction of the analyzer rotation gives the optical activity parameters.

Results and Comparison. BSO exhibits distinctive optical rotary dispersion. Figure 15 shows the values obtained for the tested samples and wavelengths versus values obtained by other experimenters with American grown material (3:131). The tested crystals all showed negative sense, although both positive and negative optical activity cry-

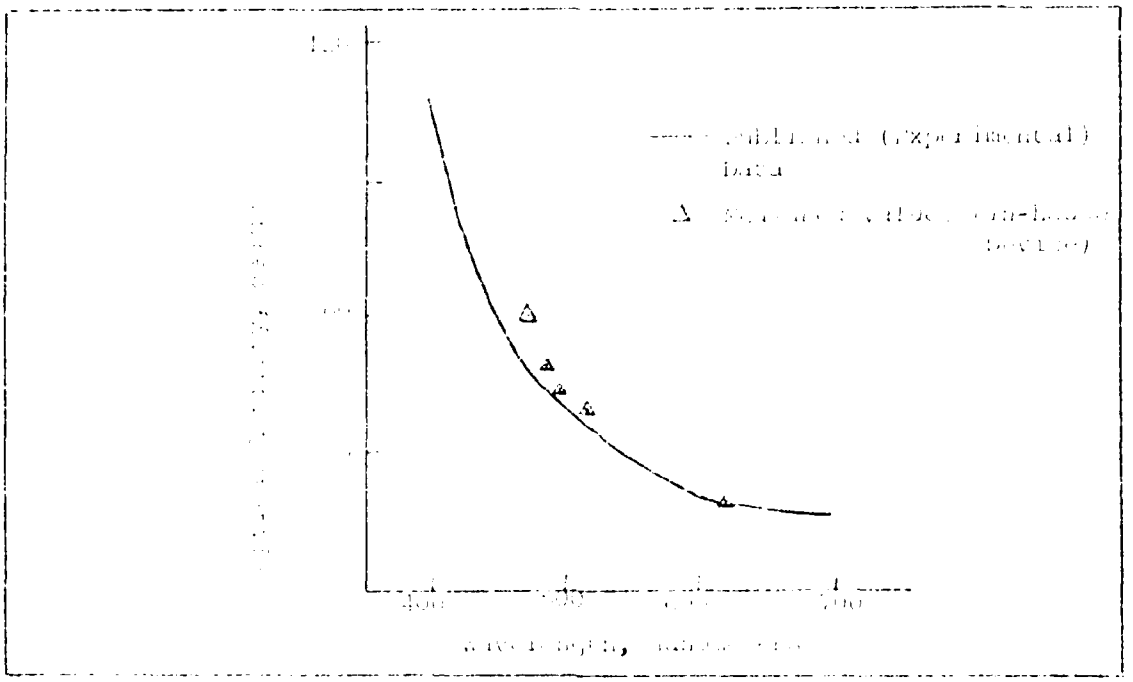

Fig. 15 Optical Activity (ρ') of BSO-Published(35:13) and Experimental

stals have been grown (1:495). The Soviet literature does not mention the sense of the optical activity for their crystals. The measured results indicate that the tested BSO samples are similar (for optical activity) to other samples.

Index of Refraction.

Experimental Apparatus. A top view of the apparatus for this measurement is shown in Figure 16. The laser beam is horizontally polarized and the screen is arranged to view the primary reflection from the crystal surface.

Experimental Procedure. The sample mount is first adjusted to insure that the laser beam is normal to the surface of the crystal. The mount is then rotated around its vertical axis and the primary reflection viewed on the screen. The rotation angle is noted when the intensity of

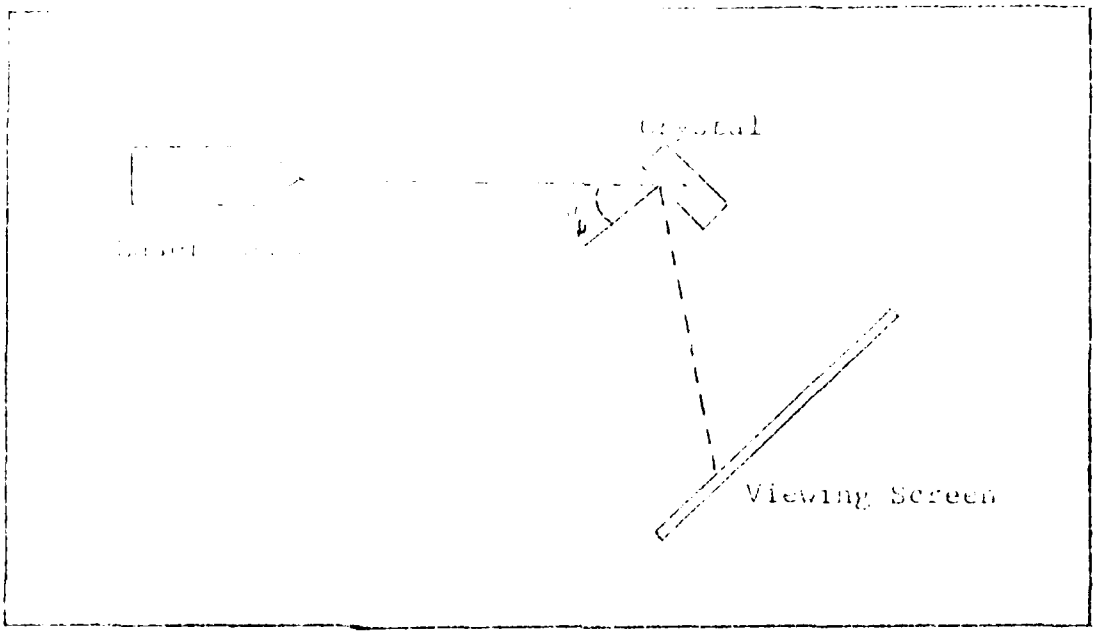

Fig. 16. Index of Refraction Measurement Apparatus

the primary reflection becomes a minimum. This procedure is repeated for each wavelength of interest.

Results and Comparison. The index of refraction measurement is based on the fact that the reflectance of linear light polarized parallel to the plane of incidence goes to zero when the polarization angle θ_p is reached. Since the relationship of this angle to the index of refraction is $n_2/n_1 = \tan \theta_p$ (19:245), the index ofrefraction of the sample can be tested. The angles measured varied from 65^0 to 70^0 which corresponds to indexes of 2.475 to 2.747. The experimental apparatus had a tolerance of $\pm 1^0$ which was not accurate enough for precise index data.Future experiments should use a more precise angular measurementtechniques. The measured data was of no use, therefore, the values listed in Table II have been assumed in future calculations.

Table II. Indexes of Refraction for BSO (35:116)

Wavelength (Å)	Index
4765	2.667
4880	2.650
4965	2.638
5145	2.615
6328	2.530

Absorption Coefficient.

Experimental Apparatus. The experimental apparatus used for this measurement is shown in Figure 17. The laser source is horizontally polarized and the crystal is tilted at 15 degrees so that the polarization of the laser is parallel to the plane of incidence with the crystal. The aperture and radiometer probe are normal to the beam propagation.

Experimental Procedure. Two data points were taken for each wavelength. The first data point consisted of the radiometer reading when the sample was not in the beam path. The second data was the reading with the crystal in place. The 15 degree tilt served to spatially separate the multiple reflections from the crystal. The aperture was adjusted to select only the primary transmitted beam for measurement.

Data Comparison. The ratio measured by this experiment is adjusted to account for reflection, surface quality, index of refraction and optical activity. The primary transmitted beam encounters a reflection, an

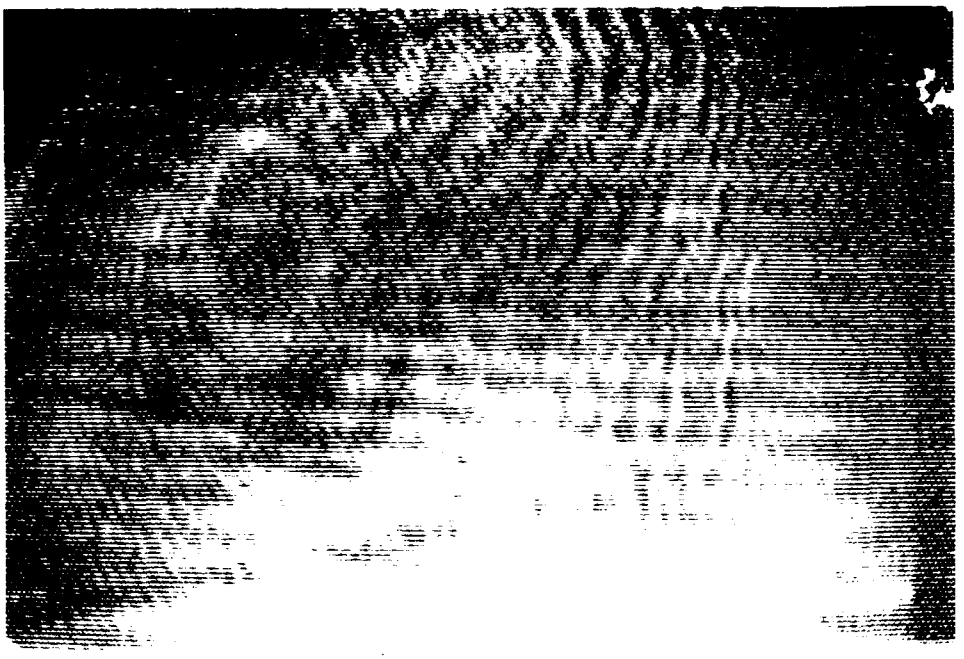

Fig. 24. Interference fringes obscuring output images

this time-changing nature, the data observed was recorded on the VTR and still photography was used to capture images from the TV screen. Resolution of fine detail, especially for a complex image, is limited due to multiple reflection, scattering, and coherent interference within the viewing optics. Detail may also be limited by the spatial resolution capability of the device, which is reported to peak at one lp/mm and usually extend to 50 lp/mm (10:195). Figure 24 shows some of the interference fringes present in the TV picture caused by coherent interference between reflections from the viewing optics.

Two different types of images were used to investigate proper image selection, a 40 um pinhole and a transparency

transient data analysis at a later date.

The power supply used to impress the longitudinal E-field is not shown in this schematic. The arrangement is identical to Figure 2 with the negative electrode on the read and write light incident side of the crystal.

Experimental Procedure. Observation of dynamic image selection is a relatively simple matter so long as the write-in image is focused on the crystal, the read beam illuminates the crystal surface, and the viewing optics are focused on the crystal surface. The procedure after the preliminary steps are complete is described below.

Shutters [9] and [15] were closed to prevent read or write light from reaching the crystal. The lasers, TV camera, VCR, and monitor were turned on and allowed to stabilize for five minutes. The power supply was also turned on, but not connected, and allowed to warm up. Once all of the equipment had stabilized, the power supply was connected and the read beam shutter [15] opened. Finally the write beam shutter was opened and an edge-enhanced version of the write-in pattern was momentarily visible on the TV screen. To further view the dynamic image selection effect, the image was moved over the crystal surface by tilting the mirror [6].

Results and Comparison. The dynamic image selection effect has been described as a reproduction or selection of the time-changing portions of an image. Because of

beam combiner [8] allows both read and write beams to be at normal incidence on the crystal. The crystal [9] is mounted on a three-axis micropositioner fabricated specifically for this experiment. The positioner facilitates viewing of any part of the crystal's back surface by the viewing optics as well as setting the optical alignment of the system.

The viewing optics consist of six primary optical elements. The microscope objective [18] is a 5.6X long working distance optic. It is followed by a Melle quarter-wave plate [19] with its fast and slow axes oriented the same as [11]. This quarter-wave plate converts the spatially phase modulated elliptical read light from the crystal to linear polarization. The analyzer [20] is oriented to provide maximum extinction to light not phase modulated by the crystal. This direction corresponds to an angle 90 degrees from the output polarization of the laser plus a correction of nine degrees for optical activity. The eyepiece [21] provides another 10X of magnification and focuses the image at a distance of about five centimeters on to the cathode of the Sony AVC-3200 video camera [23]. The 6328Å filter [22] blocks write light as well as any extraneous room light. The video camera output is passed through a Panasonic AG-6300 VCR [24] for recording to a Panasonic video monitor [25] for viewing. A Tektronics 7904 oscilloscope [26] with a 7B53A time base modified for TV field analysis is connected to allow observations of the intensity levels along any selected TV scan line. This capability is important for

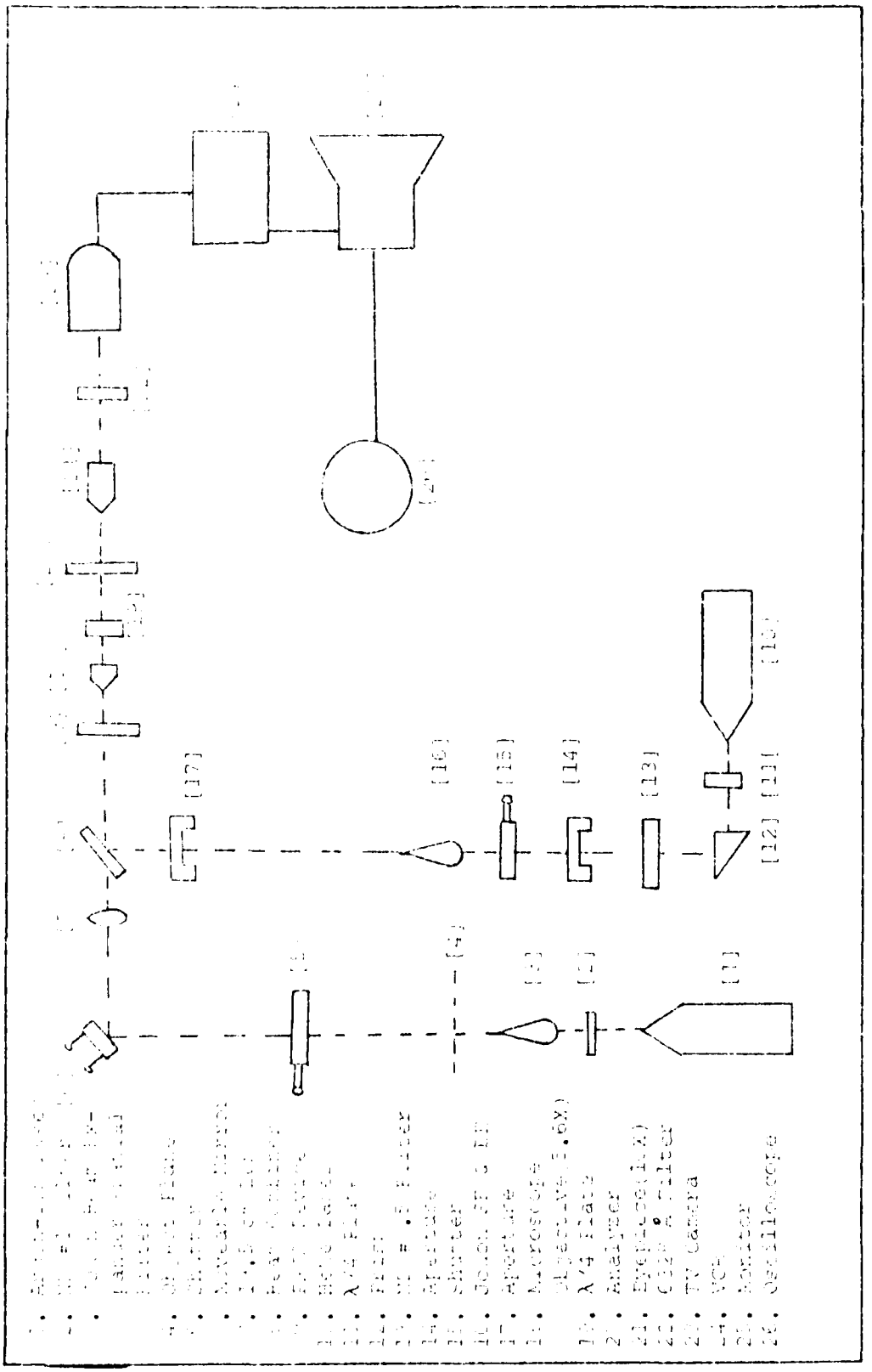

Fig. 22. Dynamic image selection experimental apparatus

[2] is necessary to reduce the irradiance of the laser to a level that will not damage the crystal. The Jodon spatial filter and beam expander [3] provide a collimated beam at the image plane [4]. The shutter [5] provides a way to control when the write beam is on the crystal. The transparency or pinhole located at the image plane is imaged through the 19.5 cm lens [7] onto the crystal surface. The mirror [6] can be tilted in two axes to allow movement of the image over the crystal surface.

The read beam path starts with the Spectra Physics 125A Helium Neon laser [10]. The quarter-wave plate [11] converts the linearly polarized HeNe beam to circular polarization. Circular polarization rather than linear polarization is used for device readout to preclude directional filtering of the input image. Directional filtering is discussed in the next section. The prism [12] uses total internal reflection to turn the beam through a 90 degree angle and maintain good beam quality. The ND #0.5 filter [13] is placed to reduce the intensity of the read beam. The aperture [14] is placed to help eliminate scattered light from the prism, quarter-wave plate, and ND filter while the shutter [15] controls the on-time of the read beam. The Jodon [16] filters and collimates the laser beam. The aperture [17] provides a method of controlling the spot size of the read beam on the crystal as well as insuring the beam is normal to the crystal surface. The

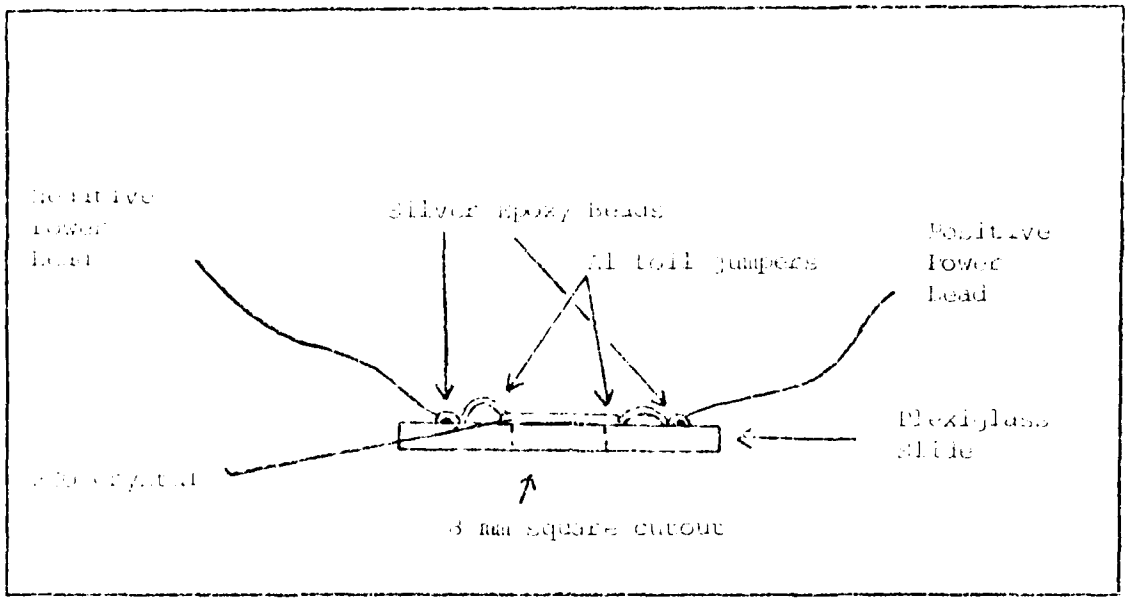

Fig. 22 Experimental DIS PRIZ Device

and protection from the handling and operating stresses of experimention. Figure 22 shows a completed current-conducting PRIZ device. Details on the mounting procedure are found in Appendix B.

Device Performance Investigation

Dynamic Image Selection. The theory and manifestation of dynamic image selection was covered in Chapter II. The lack of published material on an American device exhibiting dynamic image selection is puzzling since the results of this experiment conclusively demonstrate the effect.

Experimental Apparatus. The experimental apparatus used to investigate this parameter is shown in Figure 23.

There are two main beam paths, write and read, involved in this experiment. The write beam path starts with the Spectra Physics 162A Argon Ion laser [1]. The ND #1 filter

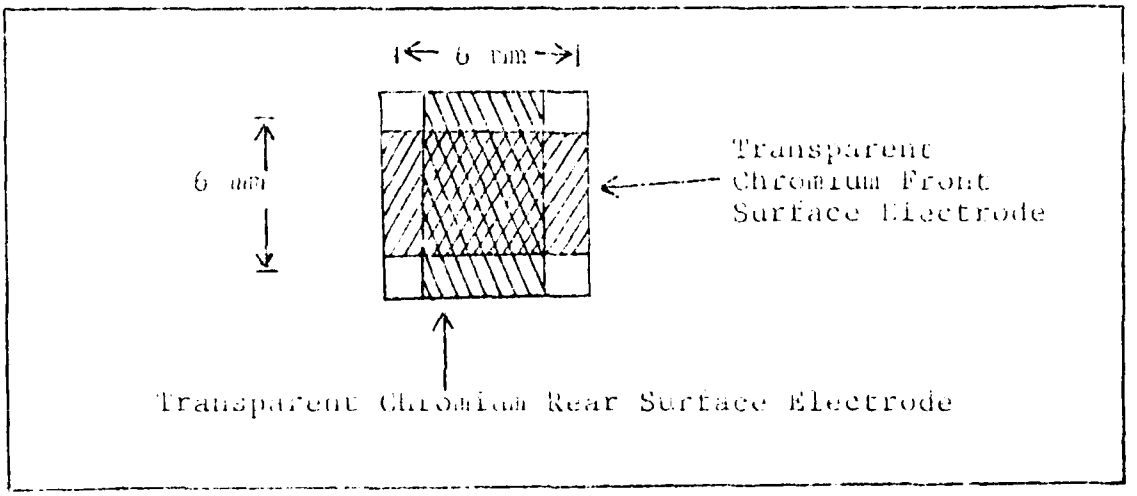

Fig. 21. Electrode Pattern Deposited on BSO Crystal

electrode application was chosen.

The electrode material chosen was chromium. There were two reasons why this material was chosen rather than those used by the Soviets. First, platinum and indium oxide were not available in sufficient quantity. Second, chromium was reported to have good adherance to BSO (35:233) as well as having good conductivity and transmissivity in very thin films (20:135).

Electrode Deposition. The BSO crystals are 1 cm square. To provide for a large active area and yet prevent shorts between the top and bottom electrodes, a 6 mm strip was deposited on each side of the crystal. The pattern is indicated in Figure 21.

Details on the deposition procedure and vacuum chamber are available in Appendix A.

Device Mounting. The BSO crystal is small and fragile. Therefore a mounting was designed to allow easy positioning

tance. The electrodes must meet three main criteria:

1. Transparent
2. Conductive
3. Good adherence to crystal

Two candidates meet these criteria, liquid electrodes and thin metal electrodes. Because of the need for good current conduction, only strong electrolytes (33:210) were considered for the liquid electrodes. The two electrolytes tested were phosphoric acid and sodium chloride solution. These liquid electrodes proved to be unsuitable for several reasons. An electrode solution of 0.5% phosphoric acid, with a conductivity of 5.5 mmho/cm caused etching of the crystal after 30 minutes. This etching changed a highly polished crystal surface into one resembling ground glass. The other solution was unsuitable because its conductivity changed with time. Under direct current, the sodium and chloride ions migrate to the anode and cathode surfaces of the circuit (35:302). This action creates a 'sheath' of ions and when tested experimentally caused a reduction in the liquid conductivity by a factor of eight. The final reason these electrodes were rejected was that they flow and evaporate.

Metal electrodes are highly conductive and nonflowing. The Soviet devices were fabricated with platinum or indium oxide electrodes that were deposited by vacuum evaporation or sputtering. A vacuum chamber was available with support equipment for evaporation deposition, so this method of

ionization at room temperature) donor concentration than that of other BSO material.

Device Construction

Design Considerations. The primary consideration in the construction of the current-conducting PRIZ, was to make an American device as similar as possible to the Soviet device. The constraints involved in this process were first, the limited construction details available in the Soviet literature, and second, the experimental and construction equipment available. The Soviet construction parameters are discussed in Chapter II.

BSO Crystal. The crystals to be used were supplied by Crystal Technology of Palo Alto, California, with the following specifications(1):

Size..... 1 cm X 1 cm

Thickness..... 0.5 mm

Flatness..... $\lambda/4$

Optical Quality

Three crystals of the (111) cut were ordered. The crystal cut selected for use in this experiment was the (111) cut because of its reported suitability for image processing (11:3351).

Electrode Selection. The electrodes used to impress the longitudinal E-field on the PRIZ were of critical impor-

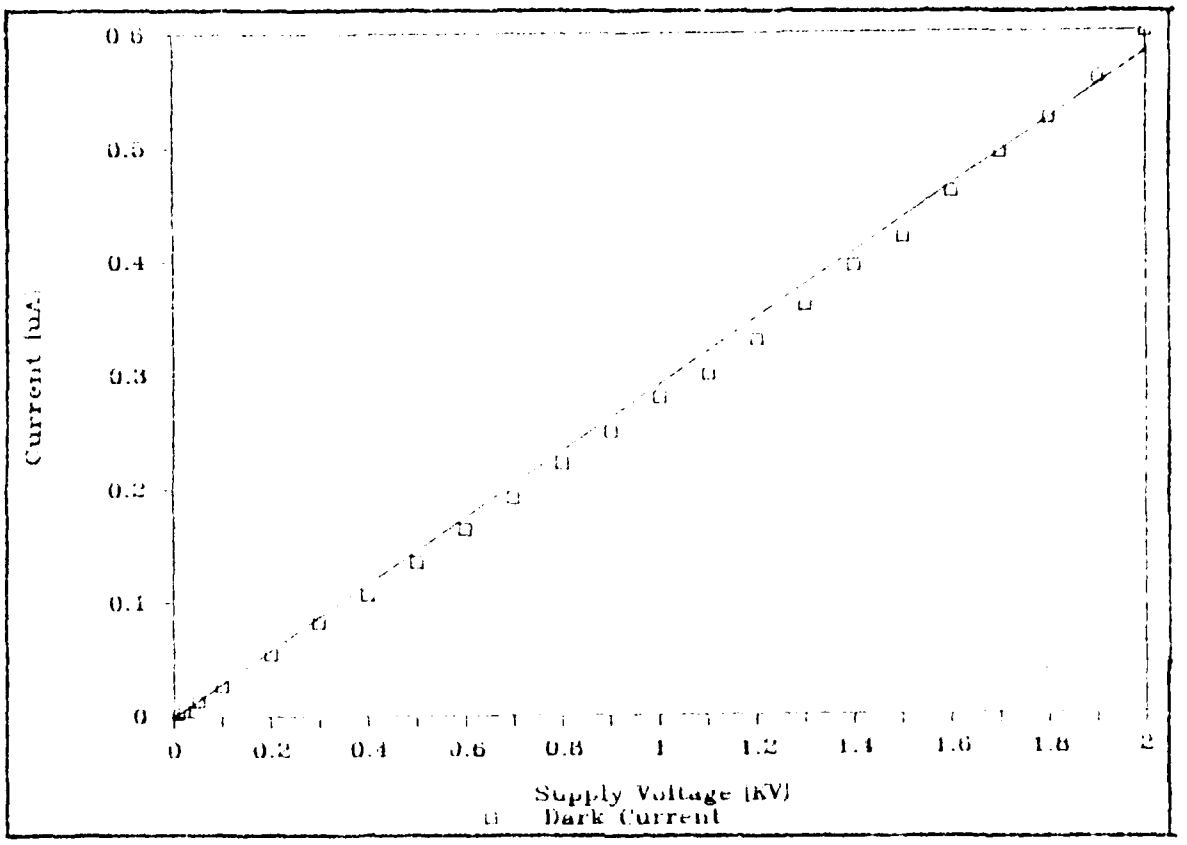

Fig. 20. Current vs Voltage Response of 550 Sample

due to capacitance in the crystal and input lines had damped out.

Results and Comparison. The device showed an ohmic current response from 10 volts to 2000 volts. Figure 20 shows the current versus voltage characteristics of the device. The slope of the graph as well as the physical dimensions of the active area of the crystal, 6 mm x 6 mm x 0.430 mm, gives a conductivity of 34.42×10^{-12} ohm^{-1} cm^{-1}. This varies significantly from the published conductivity of 20×10^{-15} ohm^{-1} cm^{-1} (2:493). This variation is believed to be due to a higher shallow (significant thermal

current through the PRIZ is a requirement of the dynamic range selection feature. The amount of current conducted under the high field (20-40 kV/cm) conditions of the current-conducting PRIZ gives important information on the donor concentration near the conduction band. The donor levels and densities drive the physical properties of the crystals and therefore the performance of the PRIZ device.

Experimental Apparatus. The experimental apparatus used to measure the dark conductivity of BSO is shown in Figure 19. The picoammeter was a Keithley 417 with a remote amplifier. The amplifier was located close to the crystal so the lead lengths were short, and hence resistances and parasitic capacitances were kept to a minimum. A Keithley 240 High Voltage Supply provided direct current to the crystal. The oscilloscope provided a method to view the transient current response of the device. The resistor acted as a current limiter to protect both the crystal and the picoammeter. Measurements were taken with the crystal in the dark to eliminate the photoconductivity contribution. The room temperature was approximately 22 degrees Centigrade although no provision was made to control or investigate this parameter.

Experimental Procedure. The voltage was set on the power supply and the current read from the picoammeter dial. A one minute wait was observed between voltage application and data reading. This wait insured that transients

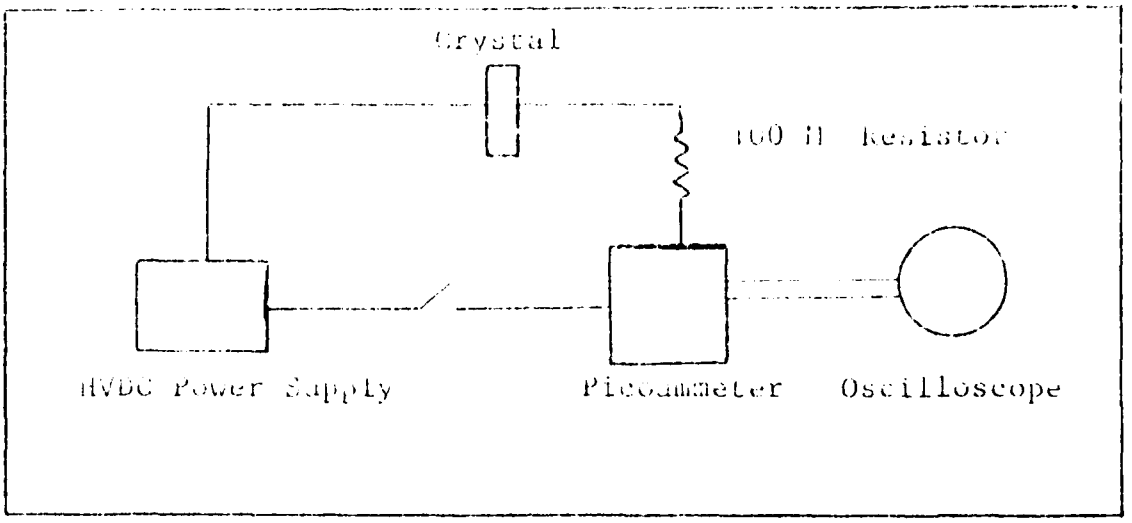

Fig. 19. Dark Conductivity Measurement Apparatus

level is associated with a silicon vacancy in the crystal lattice. Because the published and in-house measurements are equal at 2.60 eV, the donor energy level and density are considered to be characteristic of BSO. The large difference between the published and in-house measurements between 2.40 eV and 2.60 eV is assumed to be due to different levels/densities of donors/impurities. The in-house measurements ceased at 5145 Å so data between the conduction band and 2.40 eV is not shown. Because the 2.40 eV to 2.60 eV range is quite narrow (when compared to the energy band diagram of BSO, Figure 3), the variation of absorption coefficients from publish figures is not considered abnormal.

Conductivity. BSO is an semi-insulator material because of its wide bandgap and deep donor levels. However, as discussed in Chapter II, the conduction of a direct

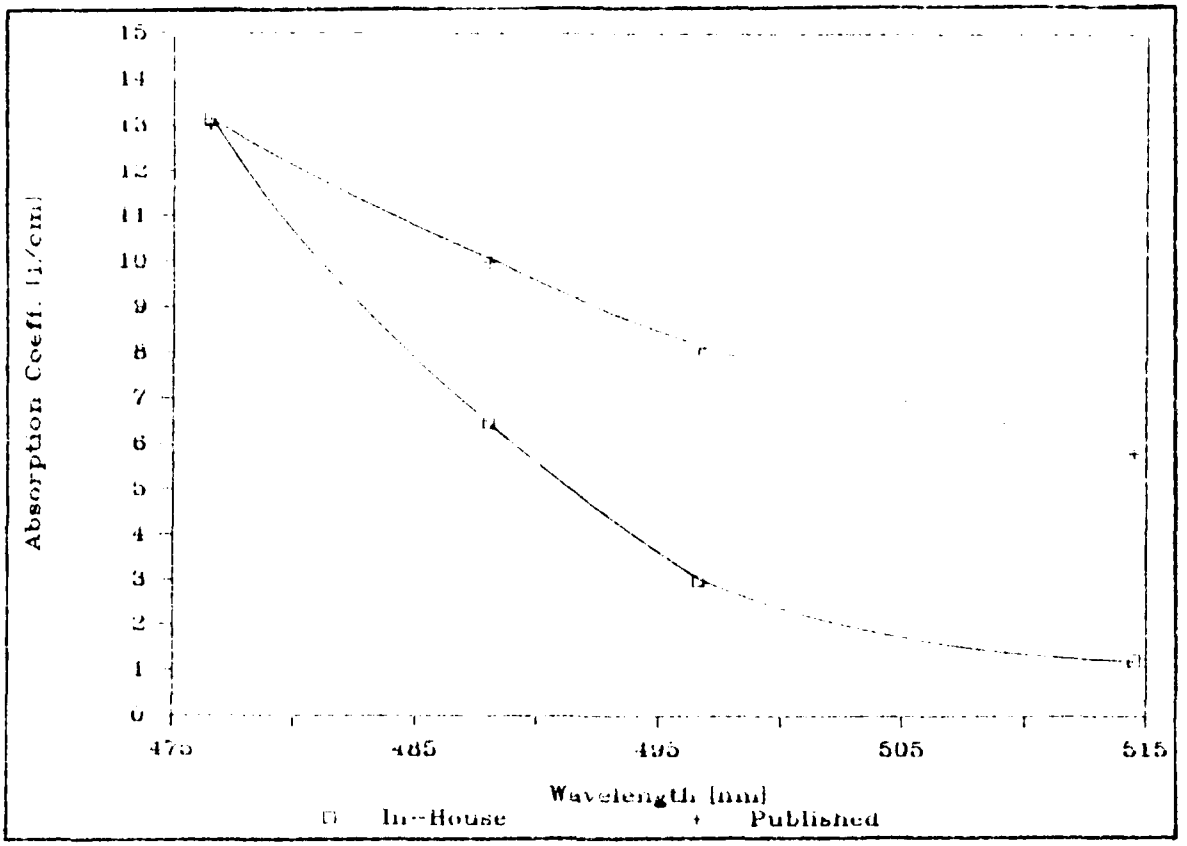

Fig. 18. Absorption Coefficient (α) vs Wavelength (λ) for B50 - Published (34:1673) and Measured Results

α is known as the absorption coefficient in cm^{-1} where d is the thickness in centimeters. With all the other factors causing attenuation of the beam accounted for, the absorption coefficient can be calculated from the experimental data.

A comparison of these results and those published for B50 are shown in Figure 18. The wavelengths available from the light source were limited to the main lines of the argon-ion laser. The data shows that the absorption coefficients for the tested material match at 4765 Å which corresponds to the 2.60 eV donor level in B50. The donor

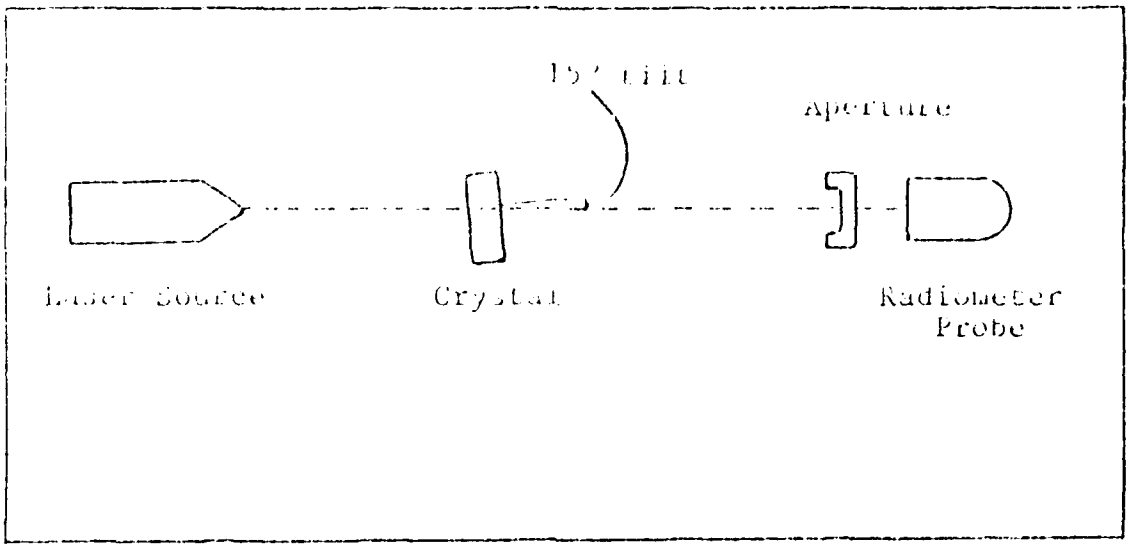

Fig. 17. Absorption Coefficient Measurement Apparatus

absorptive media, and another reflection before being measured.

The amount of light reflected from the first surface was computed using the Fresnel formula for reflection of light polarized parallel to the plane of incidence (10:75). The amount of light reflected from the second interface involved polarization components both parallel and perpendicular to the plane of incidence because of the optical activity of the crystal.

The absorption of energy in the medium can be modeled as an exponential decay of the incident intensity I_o (15:85).

$$I(d) = I_o \exp[-\alpha d]$$

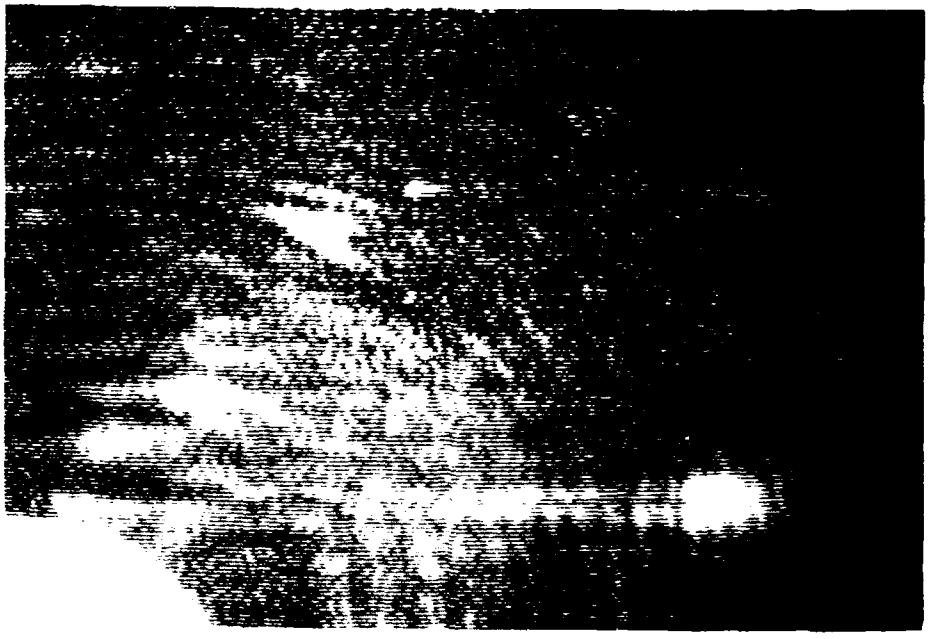

Fig. 25. Dynamic Image Retention of Moving Pinhole

of the word "GOLDEN" (1.35 mm high and 2.3 mm long). Actual size on the crystal of "GOLDEN" was 60% of original due to the magnification factor of the imaging optics. Figure 25 shows the device reproduction of the pinhole after it has been moved horizontally to the right. The bright bands of light trailing to the left are a manifestation of optical memory from the edge-enhanced sections of the image. Optical memory is explained later in this chapter. The brightest portion of the image is the leading edge. The trailing edge does not reproduce well which can be attributed to erasure by the high levels of write-light used.

A photograph of the imaged lettering is shown in Figure 26, while Figure 27 shows the device reproduction of the

Fig. 26. "CORNELL" Input Image to Current-Conducting PRIZ

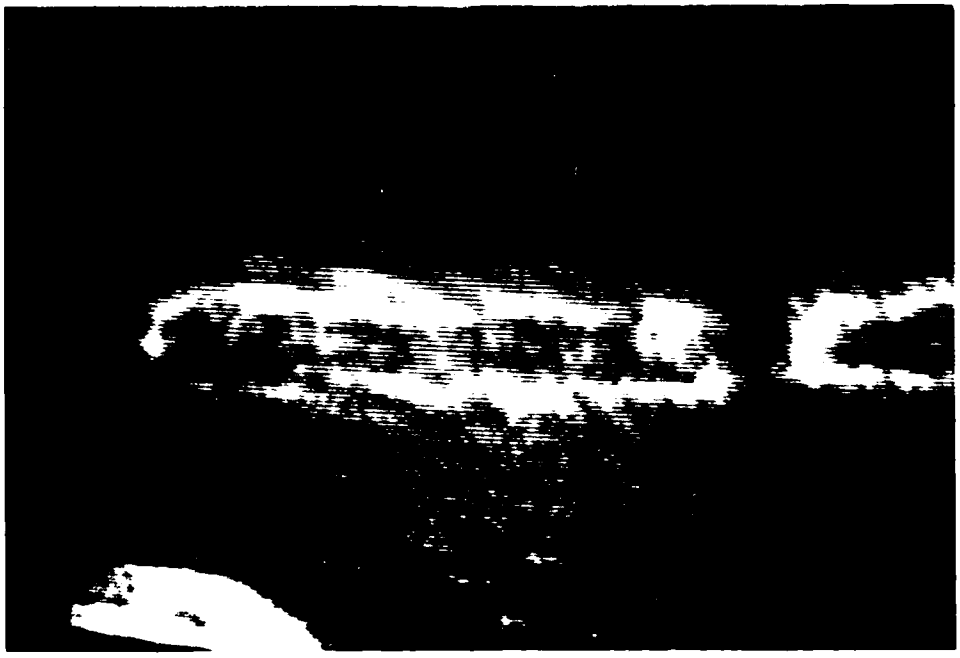

Fig. 27. Device Reproduction of "CORNELL" Input Image

"CORNELL" image. The photograph was taken approximately 0.3 seconds after write-beam turn-on. The pattern had completely disappeared by two seconds. Movement of this pattern caused increased light output along the movement track, but the image was not resolvable as letters, probably due to insufficient device spatial resolution.

The device definately shows an increased light output associated with the edges of an input image in motion. No output occurs when the image is stationary for greater than one second. These two observations are characteristic of dynamic image selection and are therefore considered proof of the effect.

Directional Filtering. Directional filtering refers to the suppression of image information that is oriented in a particular direction. The effect occurs in all versions of the PRIZ when linearly polarized light is used for device readout. The filtered direction is dependent upon the orientation of the read beam vector and the eigenvectors of the index ellipsoid. The internal transverse field $\vec{E}_t'$ associated with an edge (boundary between a light and dark area) in the write-in image will be directed normal to that edge. As indicated in Chapter II, the eigenvectors of the index ellipsoid are dependent on the direction of the transverse field. Figure 9 illustrates this fact. When the vector of the readout light $\vec{E}_R'$, defined by the angle θ", is parallel to one of the propagation eigenvectors,

only that solution will be excited. Since light output in this configuration is dependent upon a phase change between two components and the analyzer, the end result is that an edge oriented normal to the spatially filtered direction will not be reproduced.

Experimental Apparatus and Procedure. The apparatus for this experiment was identical to Figure 23 except that the quarter-wave plate [11] was replaced by a half-wave plate, and the quarter-wave plate [19] was removed. The half-wave plate allows selection of the polarization direction of the read laser which, for this experiment, was vertical. The removal of the quarter-wave plates from the read beam path causes the beam to remain linearly polarized. Linear read polarization is required for the PRIZ to exhibit directional filtering. The analyzer is oriented horizontally (plus 9 degrees for optical activity) to suppress the nondiffracted portions of the read beam. The input image [4] was a 40 μm pinhole. Intensities of the argon ion and HeNe write and read beams were set at 300 $\mu W/cm^2$. When the write beam shutter was opened, an edge-enhanced, directionally filtered version of the pinhole appeared and then faded in about a second. This image was recorded on the VCR and the orientation of the crystal recorded. Subsequent data points were taken by rotating the crystal counterclockwise around the axis of light propagation and repeating the write-in and VCR recording steps. The effect of rotating the crystal was to rotate the vector $\vec{E}_R'$ of the

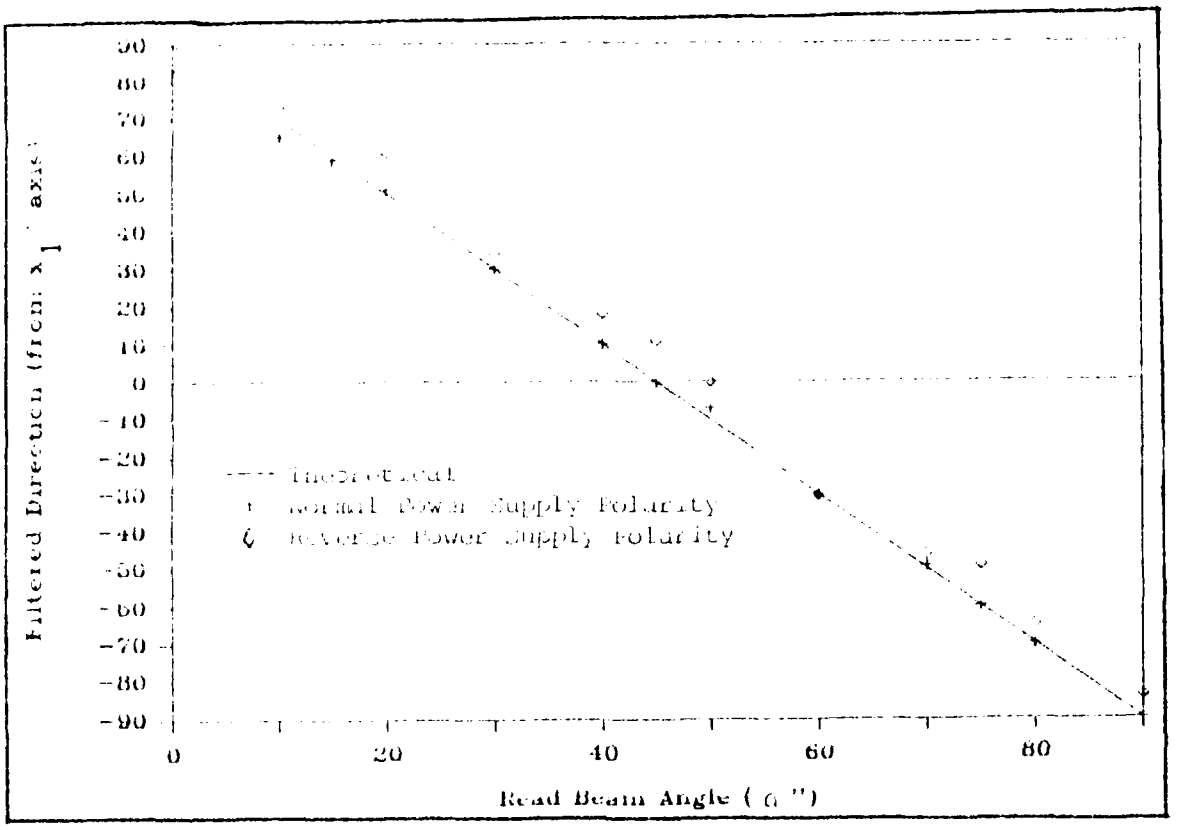

Fig. 28. Filtered Directions vs Read Beam Orientation

read beam clockwise withrespect to the crystal.

Results and Comparison. The filtered directions measured for light incident on the negative electrode agrees with the theory. Figure 28 shows experimentally measured versus theoretical values of the filtered direction for various rotation angles of the read beam vector. Soviet researchers postulate that the electrooptically active area of the current-conducting PRIZ is located near the negative electrode (25:100). Since directional filtering is dependent upon the read beam vector being parallel to one of the eigenvectors, the apparent filtered direction will shift

Fig. 29. Typical Spatially Filtered Image (Pinhole Input)

when the read beam vector is rotated due to optical activity. The second set of data points shows the filtered directions obtained when the voltage polarity on the crystal was reversed. This reversal effectively places the active area of the crystal after a volume of optically active BSO, thereby rotating the read beam vector. With light incident on the positive electrode, the filtered direction shifts an average of six degrees from the negative incidence case. This appears to verify that the electrooptically active area of the crystal volume is located near the negative electrode. A typical spatially filtered image is shown in Figure 29. This photograph is virtually identical to published Soviet results using the same type of input image (26:324).

Optical Memory. Optical memory is defined as the retention of an optical charge pattern after the write light has been removed. The storage time of this pattern is dependent on the dielectric relaxation time. In some materials, storage times of up to two years have been reported (14:229). The length of optical memory in the standard PRIZ has been previously established (11:3847) however, the duration of the memory in the current-conducting PRIZ is not mentioned in the literature. This experiment was designed to determine under what conditions the device exhibits memory and, if it does, for how long.

Experimental Apparatus. The experimental apparatus is a duplicate of that used for the directional filtering experiment, shown in Figure 23. The write-in image was once again the 40 um pinhole, and the write light power delivered was approximately 300 μW. For this experiment, the amount of energy delivered to the crystal was controlled by opening the shutter for 0.5 seconds, corresponding to 150 μJ. This energy level appeared to create the brightest spot and longest-lived image. The Helo intensity was set at 160 $\mu W/cm^2$.

Experimental Procedure. To assure that the charge pattern would not be erased by stray photogenerated electrons, the experimental area was made dark enough to consider the stray light negligible. Previous patterns were erased by exposing the crystal to a mercury penlight for one minute and then observing a two minute wait for recombina-

tion to occur. The power supply and other equipment were warmed up, stabilized and then the voltage (1000 volts) connected across the crystal. After waiting one minute for the transient currents to damp out, the write beam was pulsed on to the device. Timing for optical memory was started at this point. To check for optical memory, a read light had to be passed through the crystal. The read light was turned on after the time being checked had elapsed. If an output was visible on the TV monitor, the experiment was repeated with a longer wait time. The maximum memory time corresponded to the last visible pattern.

A second procedure used to check the memory time was to turn off the power supply after the write-in pulse. When the memory time to be checked had elapsed, both the power supply and the read beam were turned on simultaneously.

The last procedure used to check the memory time was to turn the read and write beams on simultaneously and leave the read beam on. The VCR was used to record the decay of the image.

Results and Comparison. The device demonstrates optical memory for up to 20 minutes in the dark when the power supply is left on. If the power supply is turned off after write-in, the memory time drops to around 30 seconds. The dramatic difference in these two memory times may be due to turn on/off transients in the power supply. Another hypothesis is that excess charge (electrons) is built up at

the insulator-electrode boundries of the device while direct current is flowing. Turn-off of the power supply allows the excess charge to redistribute within the bulk of the device, thus allowing recombination and hence erasure of the stored charge pattern. The maximum memory time recorded when the read beam was left on was 10 seconds. This time was recorded at 1000 volts power supply and 270 $\mu W/cm^2$ read beam intensity. The short memory time in this procedure is best explained by erasure of the pattern by the read beam. For comparison, Soviet PRIZ devices (with dielectric layers) have reported memory times of one minute in the dark and 10-20 seconds under high (2 mW/cm^2) read light intensity (11:3847). The PRIZ, however, does not conduct a direct current.

Additional Observations

Two additional phenomenon were encountered during the current-conducting PRIZ performance analysis. These phenomenon were not pursued, but their existance may be of importance to future investigators. The first phenomenon encountered was laser induced damage to the crystal and to the chromium electrodes. The second phenomenon was an oscillation in the light output from the device that was accompanied by oscillation of the current conducted through the device.

Laser Induced Damage. The BSO crystal proved to be fragile and susceptable to damage from the high fields

Fig. 30. Laser Induced Damage in BSO Crystal - Catastrophic

induced by the laser light. Figure 30 is a photograph of a hole that was inadvertently created through the face of the crystal. The field voltage was set at 1600 volts, while the Argon ion laser was set at 0.5 W/cm^2 intensity. The hole resembles the conical fracture pattern caused by a BB going through a plate glass window. The fracture starts on the negative electrode with a small ($\simeq$0.1 mm diameter) hole flaring out to a $\simeq$2 mm diameter exit hole. The most probable mechanism is dielectric breakdown of the BSO due to the high current density caused by the laser and high field. High field voltages (above 1000 V), and high write-light intensities (above 5 mW/cm^2), should be avoided to preclude this type of catastrophic damage.

Fig. 31. Laser Induced Damage in BSO Crystal - Electrode Migration

The second interesting instance of laser induced damage involved a migration of the chromium electrode material to a high field area. Figure 31 is a photograph of the pattern caused by a "CORNELL" input image. The darkening of the letters and the dendritic trails are due to chromium migration. The most interesting aspect of this occurrence is that the pattern is written on the back of the crystal. The damage occurred with the write light incident on the front electrode, the front electrode at negative potential, and the field voltage set at 2000 volts. The write light intensity was approximately 500 $\mu W/cm^2$.

Light and Current Oscillations. The phase change induced in a plane wave propagating through a current-

conducting PRIZ is dependent on the integral of the transverse field through the crystal volume. Soviet researchers have indicated that some of the solutions to this integral characteristic are oscillatory in nature. This oscillation should be observable as a flicker in a reproduced image (7:89). No Soviet experimental results were presented to support this conclusion. However, American studies of a related material, $Bi_{12}GeO_{20}$, do describe an oscillation in the current conducted through the material that is dependent on the incident light intensity and on the electric field (19:1108).

Both light and current oscillations were observed during experimentation with the current-conducting PRIZ. Steady-state light oscillations with a rate from 3 to 10 Hz were observed with corresponding current oscillations. The current oscillation occurred two to three orders of magnitude below the normal current flow due to dark current and photoelectrons. The rate of the oscillations depended on the intensity of the write light, the field voltage, and the time. For a set intensity and field voltage, the oscillation started out at a rapid pace (over 30 Hz) and then decreased to a quasi-steady value. Increasing the write light intensity of the field voltage tended to slow the oscillation rate. These observations are in qualitative agreement with the Soviet prediction. However, the Soviet researchers indicate that the oscillation is well damped, and this was not verified by this experiment. The

oscillations appeared to continue indefinately.

IV. Summary and Recommendations for Further Research

Summary

The primary aim of this study was to construct and analyze a PRIZ spatial light modulator that exhibited the dynamic image selection effect. To accomplish this aim, three main avenues were followed. These avenues were BSO material investigation, current-conducting PRIZ construction, and device performance analysis.

The BSO used in this thesis was found to be similar to that grown by other American researchers. Its optical activity and index of refraction performance matched published results. The absorption coefficients and conductivity measurements however, were different than published figures. These differences were attributed to different impurity energy levels and densities which caused lower absorption coefficients (within the range tested), and higher conductivity.

The assembled device was similar to the Soviet devices except for the electrode material and possibly the mounting technique. The chromium electrodes selected for the experimental device performed well and were relatively easy to apply. The mounting technique may have been different, but this cannot be verified because details on the Soviet technique were not published.

The performance of the experimental device for dynamic

UNCLASSIFIED

SECURITY CLASSIFICATION OF THIS PAGE

AD-A152318

REPORT DOCUMENTATION PAGE

1a. REPORT SECURITY CLASSIFICATION: UNCLASSIFIED	1b. RESTRICTIVE MARKINGS
2a. SECURITY CLASSIFICATION AUTHORITY	3. DISTRIBUTION/AVAILABILITY OF REPORT: Approved for public release; distribution unlimited.
2b. DECLASSIFICATION/DOWNGRADING SCHEDULE	
4. PERFORMING ORGANIZATION REPORT NUMBER(S): AFIT/GEO/ENP/84D-4	5. MONITORING ORGANIZATION REPORT NUMBER(S)
6a. NAME OF PERFORMING ORGANIZATION: School of Engineering; 6b. OFFICE SYMBOL (If applicable): AFIT/PH	7a. NAME OF MONITORING ORGANIZATION
6c. ADDRESS (City, State and ZIP Code): Air Force Institute of Technology, Wright-Patterson AFB, Ohio 45433	7b. ADDRESS (City, State and ZIP Code)
8a. NAME OF FUNDING/SPONSORING ORGANIZATION; 8b. OFFICE SYMBOL (If applicable)	9. PROCUREMENT INSTRUMENT IDENTIFICATION NUMBER
8c. ADDRESS (City, State and ZIP Code)	10. SOURCE OF FUNDING NOS.
11. TITLE (Include Security Classification): See Box 19	

PROGRAM ELEMENT NO.	PROJECT NO.	TASK NO.	WORK UNIT NO.

12. PERSONAL AUTHOR(S): [illegible] M. Shields, B.S., Capt, USAF

13a. TYPE OF REPORT	13b. TIME COVERED	14. DATE OF REPORT (Yr., Mo., Day)	15. PAGE COUNT
MS Thesis	FROM ______ TO ______	1984 December	82

16. SUPPLEMENTARY NOTATION

17. COSATI CODES			18. SUBJECT TERMS (Continue on reverse if necessary and identify by block number)
FIELD	GROUP	SUB. GR.	PRIZ, BSO, Dynamic Image Selection, Directional Filtering, Spatial Light Modulator
[illegible]	06		

19. ABSTRACT (Continue on reverse if necessary and identify by block number)

Title: CONSTRUCTION AND ANALYSIS OF A PRIZ SPATIAL LIGHT MODULATOR EXHIBITING DYNAMIC IMAGE SELECTION

Thesis Chairman: Theodore E. Luke

Approved for public release: IAW AFR 190-1 ... Development ... Wright-...

20. DISTRIBUTION/AVAILABILITY OF ABSTRACT	21. ABSTRACT SECURITY CLASSIFICATION
UNCLASSIFIED/UNLIMITED ☒ SAME AS RPT ☐ DTIC USERS ☐	UNCLASSIFIED

22a. NAME OF RESPONSIBLE INDIVIDUAL	22b. TELEPHONE NUMBER (Include Area Code)	22c. OFFICE SYMBOL
Theodore E. Luke	513-255-2012	AFIT/PH

DD FORM 1473, 83 APR EDITION OF 1 JAN 73 IS OBSOLETE

UNCLASSIFIED

SECURITY CLASSIFICATION OF THIS PAGE

VITA

Captain Duncan H. Shields was born 21 April 1954 in Pittsburgh, Pennsylvania. He graduated from high school in Mount Lebanon, Pennsylvania, in 1972 and entered the USAF Academy. He was commissioned a Second Lieutenant and awarded a bachelor of Science in Electrical Engineering upon graduation on 7 June 1976. He attended pilot training at Reese AFB, Texas and upon recieving his wings in July 1977, was assigned to duty as a KC-135 pilot in the Strategic Air Command. After tours of duty at Wurtsmith AFB, Michigan and McConnell AFB, Kansas, he attended Squadron Officers School at Maxwell AFB, Alabama. Captain Shields entered the School of Engineering, Air Force Institute of Technology, in May 1983.

Permanent Address: 104 Altadena Drive
Pittsburgh, PA 15228

36. Valley, George C. and Klein, Marvin B. "Optimal Properties of Photorefractive Materials for Optical Data Processing," Optical Engineering, 22 (6): 704-11 (November/December 1983).

37. Wood, Elizabeth A. Crystals and Light. New York: Dover Publications, Inc., 1977.

38. Yariv, Amnon Optical Electronics (Second Edition). New York: Holt, Rinehart and Winston, 1976.

24. Petrov, M.P. and Khomenko, A.V. "Anisotropy of the Photorefractive Effect in $Bi_{12}SiO_{20}$ Crystals," Soviet Physics Solid State, 23(5): 789-792 (May 1981).

25. Petrov, M.P. "Electrooptic Photosensitive Media for Image Recording and Processing," Proceedings of ICO-12, Current Trends in Optics. London: Taylor and Francis, 1981.

26. Petrov, M. P. et al. "Light Pulse Response of Space-Time Light Modulators using the Transverse Electrooptic Effect," Soviet Physics Technical Physics, 28 (7): 823-6 (July 1983).

27. Petrov, M. P. and Khomenko, A. V. "Physical Basis of Operation of the PRIZ Spatial Light Modulator," Optik(Germany), 67 (3): 247-56 (1984).

28. Petrov, M. P. and Khomenko, A. V. "Space-Time Modulation Characteristics of Optical Transducers," Optics Communications, 37 (4): 253-5 (15 May 1981).

29. Petrov, M. P. et al. "The PRIZ Image Converter and Its Use in Optical Data Processing Systems," Soviet Physics Technical Physics, 26 (7): 816-21 (July 1981).

30. Petrov, M.P. et al. "Transients in a Space-Time Light Modulator," Soviet Technical Physics Letter 6, (4): 165-166 (April 1980).

31. Roggeman, 2Lt Michael C. Analysis of Diffraction Efficiency of the PRIZ Spatial Light Modulators. MS Thesis, GEO 84D-6, School of Engineering Air Force Institute of Technology (AU), Wright-Patterson AFB, OH, December 1983.

32. Roggeman, M. C. and Luke, T. E. Optical Properties of $Bi_{12}SiO_{20}$. Paper Submitted for Publication. Air Force Institute of Technology (AU), Wright-Patterson AFB, OH, 45433.

33. Sienko, Michell J. and Plane, Robert A. Chemistry (Fourth Edition). New York: McGraw-Hill, 1971.

34. Sprague, Robert A. "Effect of Bulk Carriers on PROM Sensitivity," Journal of Applied Physics, 46 (4): 1673-8 (April 1975).

35. Tanguay, Armand R. Jr., The Czochralski Growth and Optical Properties of Bismuth Silicon Oxide. PhD Dissertation. Yale University, New Haven, Connecticut., 1977.

11. Casasent, David A. et al. "Applications of the PRIZ Light Modulator," Applied Optics, 21: 3846-3854 (November 1982).

12. Casasent, David A. et al. "Test and Evaluation of the Soviet PROM and PRIZ Spatial Light Modulators," Applied Optics, 20: 4215-4220 (15 December 1981).

13. Glass, A. M. "The Photorefractive Effect," Optical Engineering, 17 (5): 470-9 (September-October 1978).

14. Gunter, P., "Holography, Coherent Light Amplification and Optical Phase Conjugation with Photorefractive Materials," Physics Reports, 93 (4): 200-99 (1982).

15. Hecht, Eugene and Zajac, Alfred Optics. Reading, Massachusetts: Addison-Wesley, 1974.

16. Herriau, J. P. et al. "Some Polarization Properties of Volume Holograms in $Bi_{12}SiO_{20}$ Crystals and Applications," Applied Optics, 17 (12): 1851-2 (15 June 1978).

17. Hou, S. L. et al. "Transport Processes of Photoinduced Carriers in $Bi_{12}SiO_{20}$," Journal of Applied Physics, 44 (6): 2653-3 (June 1973).

18. Lee, S.H. Topics in Applied Physics. New York: Springer-Verlag, 1981.

19. Lenzo, P. V. "Light- and Electric-Field-Dependent Oscillation of Space-Charge-Limited Current in $Bi_{12}GeO_{20}$," Journal of Applied Physics, 43 (3): 1107-11 (March 1972).

20. Maissel, Leon I. and Glang, Reinhard eds. Handbook of Thin Film Technology. New York: McGraw-Hill, 1970.

21. McKelvey, John P. Solid State and Semiconductor Physics. New York: Harper & Row, 1966.

22. Owechko, Y. and Tanguay, Jr., A. R. "Effects of Operating Mode on Spatial Light Modulator Resolution and Sensitivity," Optics Letters, 7 (12): 587-9 (December 1982).

23. Peltier, M. and Micheron, F. "Volume Hologram Recording and Charge Transfer Process in $Bi_{12}SiO_{20}$ and $Bi_{12}GeO_{20}$," Journal of Applied Physics, 48 (9): 3683-90 (September 1977).

Bibliography

1. Air Force Institute of Technology, Air University. Purchase DD Form 1348-6 Document # R220DZ4025007610075 from Crystal Technology. Wright-Patterson AFB OH, 25 July 1984.

2. Aldrich, R. E. et al. "Electrical and Optical Properties of $Bi_{12}SiO_{20}$," Journal of Applied Physics, 42 (1): 493-4 (January 1971).

3. Astrarov, V. N. "Direct Investigation of the Electric Field Distribution in a $Bi_{12}GeO_{20}$ Crystal with the Aid of the Transverse Electrooptic Effect," Soviet Physics Solid State, 24 (1): 61-4 (January 1982).

4. Bryskin, V. V. et al. "Dynamics of Optical Image Formation in Crystals with the Aid of the Internal Transverse Pockels Effect," Soviet Physics Solid State, 24 (1): 82-6 (January 1982).

5. Bryskin, V. V. and Korovin, L. I. "Dynamics of the Distribution of Optically Induced Charges and Electric Fields in Crystals," Soviet Physics Solid State, 24 (7): 1159-62 (July 1982).

6. bryskin, V. V. et al. "Effect of Light Absorption on the Electric Field Distribution in $Bi_{12}SiO_{20}$," Soviet Physics Technical Physics, 9 (6): 686-9 (June 1983).

7. Bryskin, V. V. et al. "Initial Stage In the Redistribution of Photoinduced Charges and Electric Fields in $Bi_{12}SiO_{20}$," Soviet Physics Technical Physics, 24 (10): 1686-9 (October 1982).

8. Bryskin, V. V. and Korovin, L. I. "Nonlinear Theory of the Dynamics of the Distribution of an Electric Field in Photorefractive Crystals," Soviet Physics Solid State, 25 (1):30-3 (January 1983).

9. Bryskin, et al. "Role of Electron Injection in the Formation of Optical Images in $Bi_{12}SiO_{20}$ Crystals," Soviet Technical Physics Letters, 9 (4): 165-7 (April 1983).

10. Bryskin, V.V. et al. "Theory of Dynamic Image Selection in Photorefractive Media," Soviet Physics Solid State, 24 (2): 193-196 (February 1982).

Appendix B: Mounting Procedures

The plated BSO crystal was mounted over an 8 mm square hole in a plexiglass microscope slide. This hole was cut to keep plexiglass from interfering in the viewing path. Power supply leads were attached to the plexiglass with silver-filled epoxy and jumpered to the crystal electrodes by strips of aluminum foil. Silver circuit board paint was used to attach the foil jumpers to the electrodes on the crystal surface. The crystal was held in place on the plexiglass surface by a small drop of silver paint between the bottom electrode and the plexiglass. This drop of paint also functioned as the current path for the rear power supply jumper.

The slide was then attached to a specially fabricated 5-axis micropositioner. This micropositioner allows two degrees of calibrated translational freedom normal to the beam path and three degrees of rotation. This capability permits accurate and repeatable crystal positioning.

Vacuum Chamber Information

The evaporation chamber used was a 24-inch bell jar that was evacuated by a mechanical roughing pump and a diffusion pump with a Freon-cooled cold trap. The vacuum level in the chamber was monitored by a thermocouple gauge and a Granville-Phillips RG-75P Ion Gauge with Model 260 gauge controller. Power to the tungsten filament was controlled by a Variac connected to a 1 to 6 ratio current transformer. Gauges were installed on the secondary side of the current transformer to monitor the input power to the tungsten filament.

Appendix A: Electrode Deposition Method and Vacuum Chamber Information

Electrode Deposition Method

Deposition of the chromium electrodes on the BSO crystal was accomplished by vacuum evaporation. Sublimation of chromium occurs when it is heated above 1400° Centigrade in pressures of less than 10^{-2} torr (20:1-41). For this experiment, a 0.5 gram nugget of 99.999% pure chromium was resistively heated in a basket formed by a helically wound, single strand, tungsten filament. The vacuum pressure was 10^{-6} torr and the pellet was heated for one minute.

The electrode pattern was controlled by masking the crystal surface (leaving a 6 mm strip), and placing the masked crystal on a stage located 35.2 cm above the chromium source.

Several tests, with glass microscope slides as the target substrate, resulted in chromium films of 42% transmissivity. This uncorrected transmissivity figure was obtained by measuring the ratio of HeNe laser intensity passed by a plated versus unplated section of the slide. The transmissivity figure of 42% corresponds to a film thickness of 37 Å (35:234).

The opposite face of the crystal was plated as shown in Figure 21 to provide a central active area of 0.36 cm^2.

beam, an excellent replacement would be a broad spectrum incandescent and a series of narrow band filters. The advantages of this source would be to provide controllable input intensity in a wide selection of wavelengths.

The final area that could use improvement is the data collection and analysis equipment. Investigation of the temporal properties of the device requires a known start and stop point for events within the experimental procedure. Synchronization of the write-beam with the recording apparatus is a must for accurate time measurements. A desktop computer, such as the Zenith Z-100, with appropriate interfacing, could easily handle the timing tasks as well as any required monitoring, control, and data collection.

hopping) that most clearly reflects the operation of the device needs to be formulated. These models would be very valuable in predicting device performance and possible enhancements.

Equipment Considerations. Equipment limitations during this study played a role in the extent and quality of the recorded data. The three specific areas that need improvement are the viewing optics, light sources, and the data collection and analysis equipment.

The viewing optics caused the most noticeable problems by introducing interference and aberration into the final image. The primary method to alleviate this problem would be to use anti-reflection (A/R) coated optics in the read beam path. Another source of aberration was the organic polarizer used for the experiment. A higher quality (cosmetically as well as functionally) analyzer would do much to improve the final image. A commercially available unit is the Oriel Model 27300 Film Linear Polarizer with an A/R coating for 6328 Å.

The light sources were limited in two ways. First, the HeNe laser used for the read beam produced a poor quality (multimode, spatially inhomogeneous) beam. The use of apertures and spatial filters did not suffice to get the ideal read beam which is a plane wave of uniform intensity with controllable polarization. Second, the write-light source (Argon ion laser) was limited to four primary wavelengths. Since coherence is not an important factor for the write

results. The Soviet results are couched in terms of the diffraction efficiency which fortunately is convenient and mathematically malleable. The experiment could be configured to measure the diffraction efficiency of the device, thus providing direct comparison with the Soviet results. Gratings of various periods can be obtained with an interferometry arrangement while temporal characteristics can be investigated through write beam intensity modulation, chopping and mechanical movement.

Another area of interest is the temporal variation of the photoconductivity and light output for pulse and step inputs. The answers to these questions would provide valuable insight into the charge transport mechanism and optical transfer characteristic of the device.

Theoretical Development. A model of the dynamic image selection effect has been published by the Soviets with the caveat that it is an empirically based theory (10:196). The material and performance studies conducted in this work and suggested for further research should allow refinement of the Soviet model.

Two primary areas of theoretical development are needed. First, the three-dimensional characteristics of the internal fields generated by the photorefractive effect in the current-conducting PRIZ and the temporal nature of these fields should be investigated. Second, a charge transport model (most likely a combination of band transport and

There are four primary areas that are worthwhile in the further investigation of BSO and the current-conducting PRIZ. These areas are:

1. Additional characterization of the BSO material
2. Quantitative performance measurements on the experimental current-conducting PRIZ
3. Theoretical work on device operation
4. Equipment upgrade.

Material Characteristics. The parameters of the BSO used in this series of experiments proved to be slightly different, specifically in absorption coefficients and conductivity, than the material analyzed by other studies. A more thorough investigation of the absorption coefficients would allow selection of optimum wavelengths and intensities for any operational architecture. A suggested method would be to use a broad-spectrum light source and narrow band filters to extend the method used in this study.

The photoconductivity characteristics of the material would provide insight into the band structure and required intensity levels for desired levels of device performance. An accurate method of controlling and monitoring the input light intensity is required for good correlation with the results. A suggested method would be to use a beamsplitter so that the intensity could be continuously monitored.

Device Performance. Specific information on the spatio-temporal performance of an American built current-conducting PRIZ is needed to compare with published Soviet

image selection is qualitatively the same as the Soviet devices. The experimental device performed directional filtering in accordance with published theory and exhibited optical memory in a number of different modes.

Two interesting phenomenon encountered during experimentation, laser induced damage, and light and current oscillation were described to provide a reference for future investigators.

The dynamic image selection phenomenon that is the focus for this study represents a functional capability of prime importance. The response to the time-varying portion of an input image or two-dimensional data field represents a differentiation of that data field with respect to time (30:105). This optical data processing operation has applications in systems such as radar and missile guidance that require selection or enhancement of a signal from a constant fixed noise background (11:3854). Further study into the areas discussed above is well justified by the potential applications.

The specific objective of constructing and demonstrating a PROM that exhibits dynamic image selection was accomplished and suggestions for further research that will meet the quantitative need are covered in the next section.

Recommendations for Further Research

The purpose of this section is to suggest the research directions that I feel are most appropriate.

A PRIZ electrooptic spatial light modulator exhibiting dynamic image selection (current-conducting PRIZ) was constructed, demonstrated, and analyzed.

The current-conducting PRIZ was constructed by vacuum depositing transparent chromium electrodes on the large faces (1 cm^2) of a thin (0.5mm) slice of (111) cut Bismuth Silicon Oxide ($Bi_{12}SiO_{20}$ or BSO).

Dynamic image selection was demonstrated by writing a moving image into the device with an Argon ion laser and observing the image reproduced by a circularly polarized HeNe laser readout beam. This experiment verifies the dynamic image selection effect with a device constructed outside of the Soviet Union, an accomplishment not previously reported.

The BSO material was analyzed and found to exhibit optical activity and refractive index values similar to other American grown material. The conductivity and absorption coefficients differed significantly from the published results, being higher and lower, respectively.

The experimental device exhibits directional filtering in agreement with published theory and also exhibits optical memory times of up to 20 minutes.

END

FILMED

5-85

DTIC